To the Graduate Council:

I am submitting herewith a thesis written by David G. Whitby entitled "Wind Tunnel Support System Effects on a Fighter Aircraft Model at Mach Numbers from 0.6 to 2.0." I have examined the final copy of this thesis for form and content and recommend that it be accepted in partial fulfillment of the requirements for the degree of Master of Science, with a major in Aerospace Engineering.

Edward M. Kraft

Edward M. Kraft, Major Professor

We have read this thesis
and recommend its acceptance:

William S. Baker

Roger A. Crawford

Accepted for the Council:

Lawrence Dinkel

Vice Provost
and Dean of the Graduate School

STATEMENT OF PERMISSION TO USE

In presenting this thesis in partial fulfillment of the requirements for a Master's degree at The University of Tennessee, Knoxville, I agree that the Library shall make it available to borrowers under rules of the Library. Brief quotations from this thesis are allowable without special permission, provided that accurate acknowledgment of the source is made.

Permission for extensive quotation from or reproduction of this thesis may be granted by my major professor, or in his absence, by the Head of Interlibrary Services when, in the opinion of either, the proposed use of the material is for scholarly purposes. Any copying or use of the material in this thesis for financial gain shall not be allowed without my written permission.

Signature David G. Whitby

Date 7/26/89

WIND TUNNEL SUPPORT SYSTEM EFFECTS ON A FIGHTER AIRCRAFT MODEL AT MACH NUMBERS FROM 0.6 TO 2.0

A Thesis

Presented for the

Master of Science

Degree

The University of Tennessee, Knoxville

David G. Whitby

August 1989

ACKNOWLEDGMENTS

The author wishes to thank his major professor, Dr. Edward Kraft, and the other members of his Graduate Committee, Dr. William Baker and Dr. Roger Crawford. In addition, sincere thanks go to Mr. Earl Price and Mr. Travis Binion of Calspan Corporation for their technical review of the material presented herein.

The author greatly appreciates the efforts of Darhl Frazier, William H. Peters, and Lena Stooksbury for their preparation of figures and text. Finally, thanks are extended to the author's wife for her patience and encouragement during the hours spent earning this degree.

ABSTRACT

A wind tunnel investigation was conducted using a fighter aircraft model with various sting and blade support system arrangements to evaluate the effects of the model support system on the total body and component longitudinal force and moment data. Total aerodynamic force and moment data were determined from corrected strain gage balance measured loads. Component data (i.e. tail loads) were obtained by subtracting tail off balance data from tail on data. Data taken at free-stream Mach numbers from 0.6 to 2.0 and model angles of attack from -2 to 8 degrees were examined. The analysis indicates a significant change in total body and component force coefficients in the presence of various support system configurations. The upper blade tends to decrease drag, lift, and pitching moment coefficients, while the lower blade generally increases these coefficients. The influence of the sting on aerodynamic coefficients is a function of Mach number and angle of attack. A correction methodology using sting/blade "tares" is proposed and evaluated. The evaluation shows that total body and component force and moment coefficient data are significantly improved using sting/ blade "tares" to correct for support system effects.

TABLE OF CONTENTS

CHAPTER		PAGE
I.	INTRODUCTION	1
II.	APPARATUS	3
	Test Facility	3
	Test Article	3
	Instrumentation	4
III.	TEST DESCRIPTION	5
	Test Conditions and Procedures	5
	Corrections	6
	Data Reduction	6
	Uncertainty of Measurements	7
IV.	RESULTS AND DISCUSSION	9
	Data Presentation	9
	Total Body Loads	10
	Tail Loads	16
V.	CONCLUSIONS AND RECOMMENDATIONS	18
	BIBLIOGRAPHY	20
APPENDICES		22
APPENDIX A.	FIGURES	23
APPENDIX B.	TABLES	65
VITA		68

LIST OF FIGURES

FIGURE		PAGE
1.	Model Installation in the Transonic Tunnel	24
2.	Model Installation in the Supersonic Tunnel	25
3.	Support Configurations	26
4.	Sting and Blade Support Hardware Details	27
5.	Uncertainties of Basic Tunnel Parameters	28
6.	Support Increments	29
7.	Comparison of Support Effects, Tail On	31
8.	Comparison of Support Effects, Tail Off	39
9.	Support Correction Methodology	46
10.	Comparison of Corrections	48
11.	Tail Loads Determination	55
12.	Tail Loads Correction Methodology	56
13.	Comparison of Tail Loads and Corrections	58

NOMENCLATURE

Alpha	Model angle of attack, deg
b	Model wing span, in.
$\bar{c}$	Model mean aerodynamic chord, in.
CD	Drag coefficient for total body
CDref	Baseline total body drag coefficient
CDs	Drag coefficient due to support system
CDt	Drag coefficient for tail
CDtref	Baseline tail drag coefficient
CL	Lift coefficient for total body
CLref	Baseline total body lift coefficient
CLs	Lift coefficient due to support system
CLt	Lift coefficient for tail
CLtref	Baseline tail lift coefficient
Cond#	Number of repeat runs for a given condition
CM	Pitching moment coefficient for total body
CMref	Baseline total body pitching moment coefficient
CMs	Pitching moment coefficient due to support system
CMt	Pitching moment coefficient for tail
CMtref	Baseline tail pitching moment coefficient
DCDavg	Average drag coefficient repeatability
DCDmax	Maximum drag coefficient repeatability
DCLavg	Average lift coefficient repeatability
DCLmax	Maximum lift coefficient repeatability
DCMavg	Average pitching moment coefficient repeatability

DCMmax	Maximum pitching moment coefficient repeatability
ESP	Electronically scanned pressures
HAAS	High angle automated sting
L BLADE	Lower blade
M	Free-stream Mach number
MAX UNC	Maximum uncertainty
S	Model wing reference area, ft^2
Ualpha	Uncertainty of model angle of attack, deg
U BLADE	Upper blade
UCD	Uncertainty of drag coefficient
UCL	Uncertainty of lift coefficient
UCM	Uncertainty of pitching moment coefficient

CHAPTER I

INTRODUCTION

Current methods for supporting wind tunnel models invariably require some model geometry changes from the flight vehicle and superimpose the flow field from the support system on the model. These deviations from the flight vehicle environment can induce significant interference into the aerodynamic data. The interference varies considerably with Mach number and the type of support system used. Numerous previous investigations [1,2,3][1] indicate these phenomena for a variety of configurations. Obviously, some method for correcting force and moment data obtained in a wind tunnel must be implemented to obtain interference free model aerodynamic data for making flight vehicle performance predictions.

The purpose of this analysis is to evaluate support system effects on aerodynamic data. Specifically, the effects of an upper blade, a lower blade, and a sting on fighter aircraft model data are investigated. In addition, this thesis presents a method for correcting total body and tail load data for support system interference using support system tares and documents an evaluation of this method for various flight regimes. The method is a derivative of the tare and interference data correction method first presented by Pope [4]. It is basically linear superposition of aerodynamic data. A large number of

[1]Numbers in brackets refer to similarly numbered references in the Bibliography.

useful reports concerning support interference of wind tunnel models is listed by Tuttle and Gloss [5]. They present a thorough bibliography of works pertaining to support interference.

Comparisons of support increments, tail loads, and the correction methods are presented for Mach numbers 0.6, 0.8, 0.9, 1.2, 1.5, 1.6, 1.8, and 2.0 and angles of attack -2, 0, 4, and 8 degrees.

The purpose of this thesis is to reveal conclusions with regard to support system interference using only the applicable data obtained during the tests described in Chapter III. Therefore, this thesis does not fully detail the subject tests and presents data only in incremental form.

CHAPTER II

APPARATUS

Test Facility

The tests were conducted in continuous-flow closed-circuit transonic and supersonic wind tunnels. The test sections are 16-feet square by 40-feet long. The transonic test section is enclosed by 60-deg inclined-hole perforated walls of six-percent porosity, and the general arrangement of the test section and the test article is shown in Figure 1.[1] The supersonic test section and test article arrangement is shown in Figure 2.

Test Article

The test article was a scale model of a fighter aircraft. The model was supported by either a sting or an upper or lower blade arrangement. In addition to the three main support systems, a dummy sting or a dummy blade was attached to the upper blade supported configuration to evaluate the aerodynamic influence of each support type on the model. Each support system configuration was attached to the facility High Angle Automated Sting (HAAS) support system in the transonic wind tunnel and the High Pitch Sting Support System in the supersonic wind tunnel. A representation of the model with the lower blade support configuration is shown installed in the transonic tunnel in Figure 1 and in the supersonic tunnel in Figure 2. Each of the

[1]Figures are presented in Appendix A.

model support arrangements is shown in Figure 3, and sting and blade support hardware details are shown in Figure 4.

The support systems shown in Figure 3 are all non-metric, so the loads associated with the supports are not measured. Only their influence on the aircraft model and model loads are measured. This arrangement results in a metric/non-metric break which must not be bridged in order not to obtain fouled balance data. The metric/non-metric clearance must be designed large enough based upon balance deflections so that the balance does not foul.

Model aerodynamic data were corrected for flow-through duct drag and for model base and cavity pressure tares. The sting shroud was a metric model component (i.e. the balance sensed the loads associated with the shroud), and it is shown surrounding both the sting and dummy sting in Figure 3.

Instrumentation

A six-component strain gage balance was used to measure aerodynamic forces on the model. The balance outputs were recorded on the facility data acquisition systems and transmitted to the facility computer for calculation of corrected force and moment coefficients.

The model surface, cavity, internal flow duct, and base pressures were measured by three 15-psid, 48-port ESP modules.

The model pitch angle was determined from standard HAAS and high pitch system instrumentation and verified by a Schaevitz angular position indicator located in the model. Thermocouples were used to monitor the temperature of the balance and the ESP transducers.

CHAPTER III

TEST DESCRIPTION

Test Conditions and Procedures

For the current study, data were obtained at free-stream Mach numbers of 0.6, 0.8, 0.9, 1.2, 1.5, 1.6, 1.8, and 2.0 at a constant unit Reynolds number of 2.0×10^6/ft in the transonic tunnel and 1.5×10^6/ ft in the supersonic tunnel.

Data were obtained by establishing the appropriate test section flow conditions and model attitude (model angles of attack used in this report are -2, 0, 4, and 8 degrees) and recording steady-state data. The variation of model angle of attack, and data acquisition were computer controlled.

All steady state measurements were sequentially recorded by the facility on-line computer system, which reduced the data to engineering units, further processed the data to obtain the required model parameters, tabulated the data in the tunnel control rooms, recorded the data on digital magnetic tape, and transmitted the data to the central computer file. The data stored in the central computer file were generally available for plotting and analysis with the Interactive Graphics System within 30 seconds after data aquisition. The immediate availability of the tabulated and plotted data permitted continual on-line monitoring of the test results.

Corrections

The balance-measured forces and moments were corrected for sensed changes in model weight, model base and cavity pressure forces, and internal duct flow forces. Upper and lower blade cavity pressures were used to correct normal force and pitching moment coefficients. Upper blade cavity pressures were also used to correct axial force since some slope existed on the upper surface of the model.

The sting support configuration used a metric shroud to smoothly fair the portion of the model where the sting entered. Balance data were corrected for shroud base and cavity drag but not for normal force or pitching moment resulting from this shroud. Since it was a metric component but did not represent true geometry, the shroud is thought to have introduced some error which was not corrected for in normal force and pitching moment. Model pitch angle was corrected for flow angularity in both wind tunnels. Because of the relative cross-sectional areas of the model/support system and test section, tunnel blockage and wall interference effects are assumed negligible.

Data Reduction

The facility standard force and moment data reduction program was used to compute model aerodynamic loads from balance outputs. The corrected balance forces were converted to body and stability axes coefficients based on model wing reference area (S), wing span (b), and mean aerodynamic chord ($\bar{c}$).

Exit plane rake pressures were used to calculate internal duct drag for the flow-through ducts. Model pressures were reduced to

coefficient form based on free stream conditions. Pressure substitution and bad-coding were provided when measured pressures were not available or deemed incorrect. The total aerodynamic loads on the model were obtained by summing the balance measured loads and the appropriate tare loads and corrections.

Model attitude was calculated from measured sting support pitch and roll angles with corrections for balance/sting angular deflection and wind tunnel flow angularity.

Uncertainty of Measurements

Uncertainties (combinations of systematic and random errors) of the basic tunnel parameters, shown in Figure 5, were estimated from repeat calibrations of the instrumentation and from the repeatability and uniformity of the test section flow during tunnel calibration. Uncertainties in the instrumentation systems were estimated from repeat calibrations of the systems against secondary standards whose uncertainties are traceable to the National Bureau of Standards calibration equipment. The tunnel parameter and instrument uncertainties, for a 95% confidence level, are combined using the Taylor series method of error propagation described by Abernethy [6] to determine the uncertainties of the reduced parameters shown in Table 1[1] for selected test conditions.

Repeatability of data used for this investigation is shown in Table 2. Both maximum repeatability values and average repeat data

[1]Tables are presented in Appendix B.

based on the number of repeat runs for a given condition are presented. Generally the repeatability values are somewhat less than the data uncertainty at the corresponding test condition. Occasionally, however, the repeatability is more on the order of twice the uncertainty. Repeat comparisons using data obtained at the very start of testing in each wind tunnel are included, and it is assumed that installation effects and balance zero shifts are the major contributors when such large repeat data discrepancies occur.

CHAPTER IV

RESULTS AND DISCUSSION

Data Presentation

For this analysis, data were obtained with the five support system configurations shown in Figure 3. Drag, lift, and pitching moment coefficients for the configurations were then subtracted as illustrated in Figure 6 to obtain support increments for both tail-on and tail-off configurations for each of the three main support configurations.

The computer program used to obtain data increments fits drag, lift, and pitching moment coefficients as functions of angle of attack using a least squares, third order polynomial curve fit. The program then calculates increments at specific angles of attack from the curve fits. The increments are plotted in Figures 7-8. The same method was used to obtain repeatability values at discrete angles of attack (see Table 2).

Data for the five configurations in Figure 3 were also obtained at discrete angles of attack from the curve fits. These data along with the support increments described above were then combined as shown in Figure 9 resulting in corrected data. The five support corrections are evaluated relative to a baseline or reference correction. For comparing support increments in this study, data derived from Case 1 (see Figure 9) are defined as the baseline. Case 1 reference data were

subtracted from data for each of the other cases. The five sets of corrected data are presented relative to the baseline data in Figure 10.

Tail loads were obtained using an incremental method shown in Figure 11. Two tail increment corrections ("lower blade corrected" and "sting corrected") were employed by combining data from various configurations as shown in Figure 12. The data plotted in Figure 13 represent both the corrected and uncorrected (influenced by the support system) tail loads. Similar to the presentation of total body loads, tail loads are plotted referenced to a set of baseline data. For Figure 13, the baseline data are the "lower blade corrected" data.

Total Body Loads

Support System Increments. The contribution of the support configuration to the total body lift, drag, and pitching moment coefficients is shown in Figures 7-8. Force and moment coefficients are plotted as a function of Mach number for both the tail-on configurations (Figure 7) and tail-off configurations (Figure 8). Each figure consists of drag, lift, and pitching moment coefficient plots. The Mach number scale on the abscissa is split at M = 1.6 which is repeated. Data at Mach number 1.6 were obtained in both wind tunnels, and each data set is presented.

A comparison of the drag coefficient data from the two blade configurations indicates that the lower blade generally has the larger effect which is to produce a higher drag coefficient. The upper blade

often has the effect of decreasing drag coefficient especially subsonically. At low angles of attack (alpha = -2 and 0 degrees), the difference between the effects of upper and lower blade on drag coefficient is moderate (less than 0.0020) subsonically and low (less than 0.0010) supersonically. As model angle of attack is increased to 4 and 8 degrees, the difference between upper and lower blade effects increases considerably at Mach numbers between 0.9 and 1.2. Though the magnitude of the blade effects is a function of angle of attack, the directions of the effects generally remain consistent as angle of attack changes.

The sting's effect on total body drag coefficient is a strong function of both Mach number and angle of attack. At low angles of attack, the sting decreases drag coefficient even more than the upper blade, while at higher angles, it increases drag coefficient more than the lower blade. The sting and shroud effectively pressurize the lower surface through which they enter the model yielding a decrease in drag coefficient at negative angles of attack and an increase in drag coefficient at positive angles. The effects are the same in direction across the Mach number range, but they are significantly larger at supersonic Mach numbers.

Upper and lower blades produce nearly equal decreases and increases in lift coefficient respectively. Subsonically, the blade lift coefficient increments are nearly symmetric about the x-axis. The blades act as spoilers, pressurizing the surfaces through which they enter the model. The differences between upper and lower blade

increments are small at Mach number 0.6, but at Mach numbers above 0.6, the differences increase significantly.

The sting lift coefficient increments are high positive values relative to those of the lower blade for all Mach numbers and angles of attack. Lift coefficient was not corrected for the metric shroud surrounding the sting, therefore these results are explained by the sting shroud acting as a flap deflected positively to increase lift.

It is interesting to note that lift coefficient increment signs and magnitudes for each support configuration are nearly independent of angle of attack. This observation is in contrast to the large angle of attack effects measured for drag coefficient.

Upper and lower blades also produce nearly equal decreases and increases in pitching moment coefficient respectively. The pitching moment coefficient increments for Mach numbers up to 1.6 are practically symmetric about the x-axis. The differences between upper and lower blade increments are nearly constant at subsonic Mach numbers and decrease steadily as supersonic Mach number increases.

The increase/decrease in pitching moment coefficient with a corresponding increase/decrease in lift coefficient indicates that the major influence of the strut is to pressurize the model surface in front of the model's center of pressure.

The sting produces a very small pitching moment coefficient increment subsonically and a distinctly negative increment supersonically. Therefore, it is concluded that at subsonic Mach numbers, the interference region of the sting is essentially centered about the

model center of pressure. Even though the model center of pressure shifts aft at supersonic Mach numbers, the interference region of the sting at these Mach numbers is centered even farther aft causing a negative increment in pitching moment coefficient.

As with the lift coefficient, pitching moment coefficient increments for each support system arrangement are practically independent of model angle of attack.

Comparing data in Figure 7 with the corresponding data in Figure 8, the tail seems to have no effect on the sign of support effects. The magnitude of the support increments is very similar but generally smaller in the absence of the tail. This observation leads to the conclusion that the support increments described above tend to be independent of small changes in configuration.

The tendency for the direction of sting and blade increments to be configuration independent is reinforced by the data contained in reports by Carter [2] and Wells [3]. Lower blade and/or sting arrangements, similar to that used during this investigation, were used for two cargo/transport configurations at subsonic Mach numbers. The effects of the support systems on drag and pitching moment coefficients shown in these reports are consistent with the corresponding effects in this study.

Even though the effect of the support system on the sign of longitudinal force and moment coefficients is consistent between the three configurations, the magnitude of support increments varies between configurations. Figures 7 and 8 show a large influence of

support system on aerodynamic coefficients (relative to the uncertainty) which must be removed from the data to achieve accurate information.

Correction Methodology. To account for the appreciable effects of the support system described above, a set of corrections using sting/blade "tares" is proposed and evaluated. The five cases which were applied to the data in this thesis are shown in Figure 9. Logically, a sixth case using the upper blade tail-on configuration would follow, but this method would be identical to Case 1.

Each of the cases in Figure 9 was applied to the uncorrected data base to obtain total body loads with support system interference tares removed. The support system tare correction methodology is evaluated by checking how well and for which conditions the five cases agree.

As described in the data presentation section of this chapter, the baseline (Case 1) data were subtracted from data for each of the other cases. For this reason, the abscissa is actually one of the five cases for the purposes of Figure 10. The "Figure of Merit" used to evaluate correction method agreement is ± the uncertainty (effectively twice the uncertainty). The uncertainty bands shown in Figure 10 are only those associated with absolute aerodynamic coefficient data and not incremental data. Without knowledge of the magnitude of aerodynamic coefficients deemed significant to impact aircraft performance, this uncertainty band represents only a "Figure of Merit" to evaluate the correction methodology. For the purposes of this thesis, the uncertainty band is an arbitrary basis for comparison of corrections. Since the

baseline correction was chosen arbitrarily and is not necessarily the correct answer, the uncertainty band is moved to surround as much of the data as possible.

A comparison of Figure 10 with Figures 7-8 reveals that differences between sets of corrected drag coefficient data are significantly less than the corresponding support interference increments. For example, the average absolute support increment in drag coefficient at alpha = 8 degrees with the tail on is 0.0026 (see Figure 7d), but the average deviation of the corrected data from baseline data is 0.0012 for the same conditions (see Figure 10d). In fact, at low angles of attack (alpha = -2, 0, and 4 degrees), the five cases agree to within the uncertainty band described above. At 8 degrees angle of attack, only the subsonic Mach number data agree well enough to conclude that the cases converge to the correct drag coefficient.

Although some lift coefficient data fall outside the uncertainty band for Mach numbers between 0.9 and 1.6, the corrected data agree better than the magnitude of the original support increments. Using alpha = 8 degrees with the tail on as an example, the average absolute support increment in lift coefficient is 0.0117 (see Figure 7d), while the average deviation of corrected data from the baseline data is 0.0051 (see Figure 10d).

For pitching moment coefficient, the five cases agree better than the magnitude of the support increments again, but nowhere does the correction method collapse all data to within the uncertainty band described above. Especially at Mach number 1.2, the support increments

do not collapse to within data uncertainty, but a considerable improvement of the data is still observed. For example, at alpha = 8 degrees with the tail on, the average absolute support increment in pitching moment coefficient across the Mach number range is 0.0084 (see Figure 7d), while the average deviation of corrected data from the baseline data is 0.0034 for the same conditions (see Figure 10d).

Tail Loads

Support System Effects. The effect of the upper blade, lower blade, and sting support configurations on tail loads was investigated by subtracting test data as shown in Figure 11. The data represented by the open symbols in Figure 13 are referenced to a baseline (see the data presentation section of this chapter). The closed symbols in Figure 13 represent corrected tail load data which will be discussed in the next section. Effects of support system on tail drag coefficient exist, but they are on the order of the data uncertainty. Tail lift coefficient increments due to the support system are slightly greater than data uncertainty especially at Mach number 1.2. Tail pitching moment coefficient increments fall outside the data uncertainty band at all Mach numbers with the largest effect at Mach number 1.2. The effects increase slightly as angle of attack increases.

Correction Methodology. Two cases shown in Figure 12, "lower blade corrected" and "sting corrected", were used to obtain corrected tail load data. The corrected tail loads based on the two cases are shown along with the tail loads in the presence of the support system

in Figure 13. The format and scales for these figures are identical to those of Figures 7, 8, and 10. The "lower blade corrected" case was used as a baseline and is therefore represented by the abscissa. The evaluation of the support tares method of correction is again based upon the agreement of the two corrections in Figure 12. In Figure 13, the abscissa and the closed circles represent these two corrections, so the degree to which the closed circles follow the x-axis is a measure of the consistency of the correction method.

Even though the data in the presence of the support system are often inside the uncertainty band themselves, the corrected data agree significantly better than the uncorrected tail support increments. The closed circles in Figure 13 nearly always fall to within the arbitrary uncertainty band of the abscissa (pitching moment is the best example).

CHAPTER V

CONCLUSIONS AND RECOMMENDATIONS

An analysis was conducted to evaluate support system interference using a fighter aircraft model. Various support system configurations were used with appropriate dummy sting and blade models to assess the influence of an upper blade, a lower blade, and a sting on the longitudinal aerodynamic coefficients and tail loads of an aircraft model. Appreciable support system effects are found to exist for both total body and tail loads. In general, the upper blade decreases drag, lift, and pitching moment coefficients, and the lower blade increases the coefficients. The sting's effect on forces and moments varies significantly with Mach number and angle of attack.

A correction methodology using support "tares" is presented and evaluated. Several combinations of support tares were applied to the wind tunnel data. The corrections are evaluated by examining how well and for which conditions they agree. The basis used for this comparison is the absolute aerodynamic coefficient uncertainty, which is only an arbitrary "Figure of Merit". This analysis shows that drag coefficient can be significantly improved using sting/blade tares except at supersonic Mach numbers at high angles of attack. This result suggests that minimum drag data could be one application for the use of support tares to correct for support system effects. Although lift coefficient corrections do not collapse to within the data uncertainty for all Mach numbers, and pitching moment coefficient corrections rarely collapse

based on data uncertainty and repeatability, lift and pitching moment data are improved by applying support tares. Failure of the correction methodology to collapse all the data is attributed to several factors. The first of the factors are the basic limitations embedded in the sting/blade tares methodology which would include secondary effects such as mutual interference between the actual and dummy support systems and non-linear flow effects such as flow separation from the model surface. Also contributing to lack of agreement are installation effects from installation and removal of the various configurations and temperature effects resulting in balance shifts which could not be controlled.

A similar correction methodology was applied to tail force and moment coefficients. In this case, drag, lift, and pitching moment coefficient corrections were found to collapse to within the data uncertainty described above.

At the conditions for which the cases collapse, any one of the correction cases can be chosen to properly correct aerodynamic wind tunnel data. Obviously, less time and expense are required to use the correction cases with only three configurations rather than those cases requiring five configurations. The best method for reducing support system interference is a magnetic suspension and balance system. As this technology is developed it should be used more frequently, since the method has no support interference and thus requires only one configuration.

BIBLIOGRAPHY

BIBLIOGRAPHY

1. Alstatt, M. C. and Dietz, W. E. "Support Interference on an Ogive-Cylinder Model at High Angle of Attack in Transonic Flow." AEDC-TR-78-8 (AD A051689), March 1978.

2. Carter, E. C. "Interference Effects of Model Support Systems." AGARD-R-601, April 1975, pp. 3-1-3.10.

3. Wells, O. D. et. al "Preliminary Analysis of the C-17A Phase II Configuration Development Model Test in the Rockwell International 7-Foot Trisonic Wind Tunnel." Douglas Aircraft Company Report MDC J9517.

4. Pope, Alan. Wind Tunnel Testing. John Wiley and Sons, Inc., New York, 1958 (Second Edition).

5. Tuttle, Marie H. and Gloss, Blair B. "Support Interference of Wind Tunnel Models - A Selective Annotated Bibliography." NASA Report TM81909, March 1981.

6. Abernethy, R. B. and Thompson, J. W., Jr. "Handbook - Uncertainty in Gas Turbine Measurements." AEDC-TR-73-5 (AD755356), February 1973.

APPENDICES

APPENDIX A

FIGURES

This appendix presents Figures 1 through 13 cited in the main text.

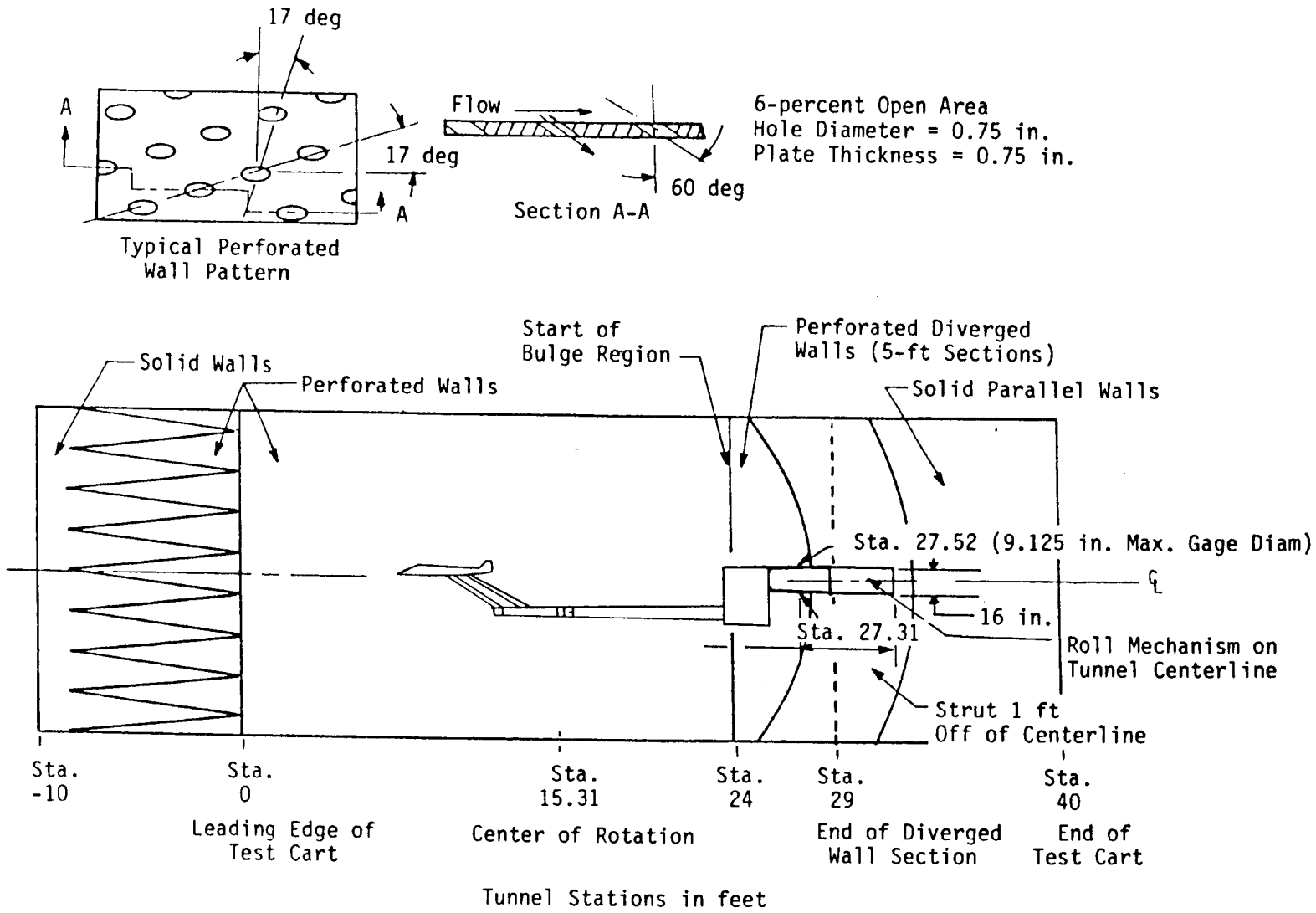


Figure 1. Model Installation in the Transonic Tunnel

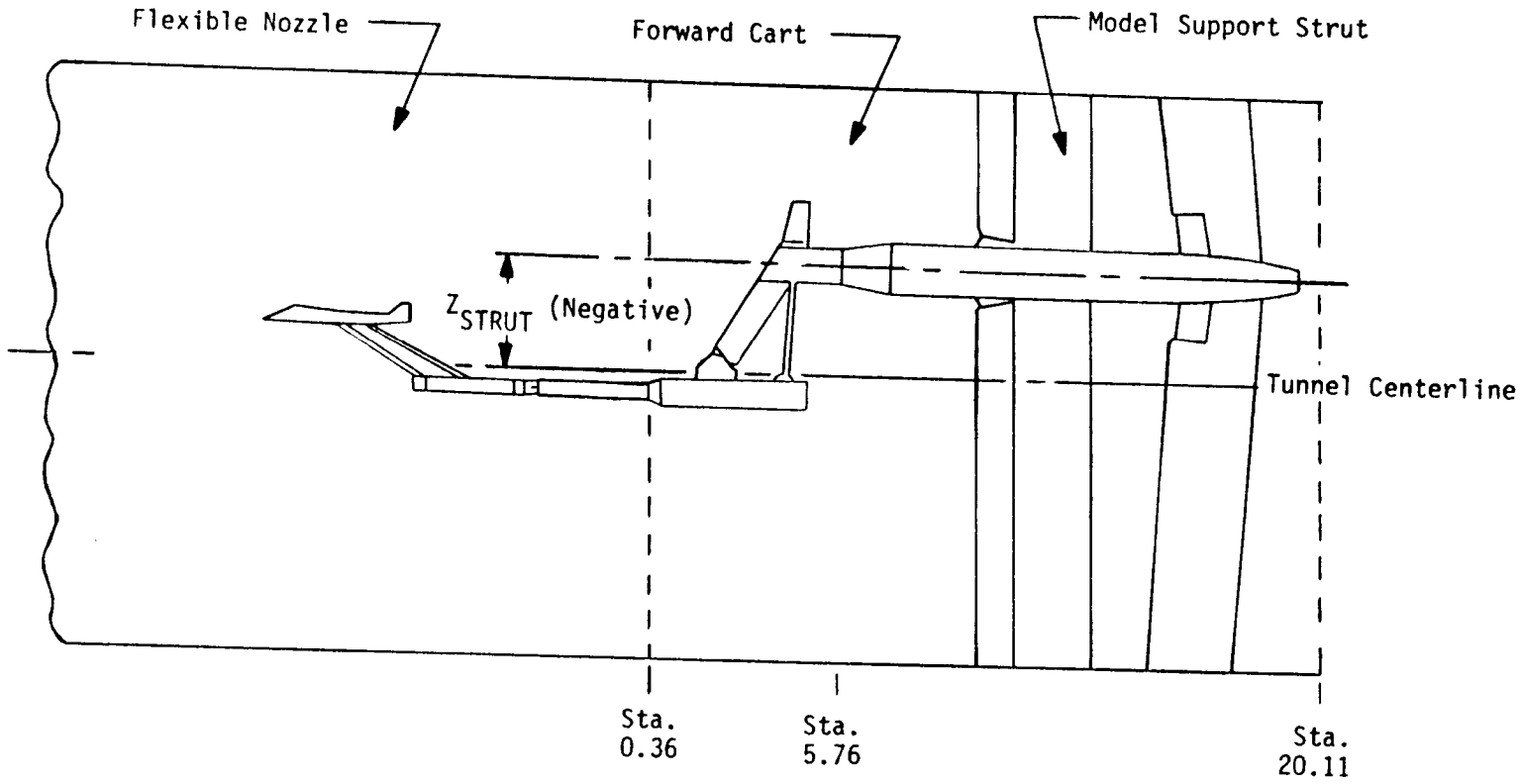
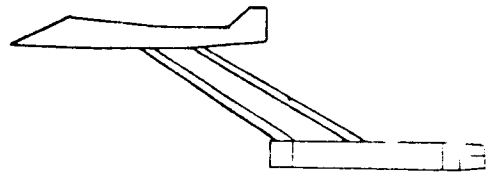
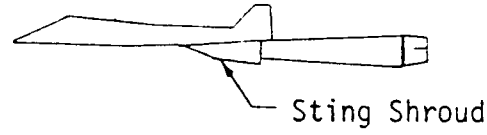


Figure 2. Model Installation in the Supersonic Tunnel

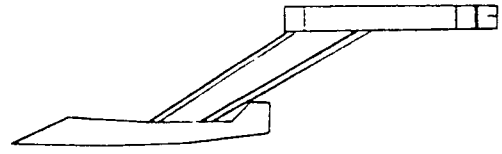
Lower Blade



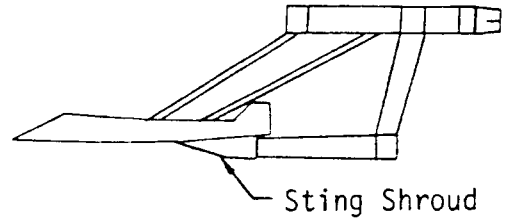
Sting



Upper Blade



Upper Blade, Dummy Sting



Upper Blade, Dummy Lower Blade

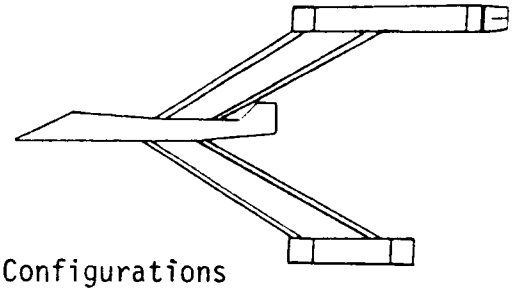
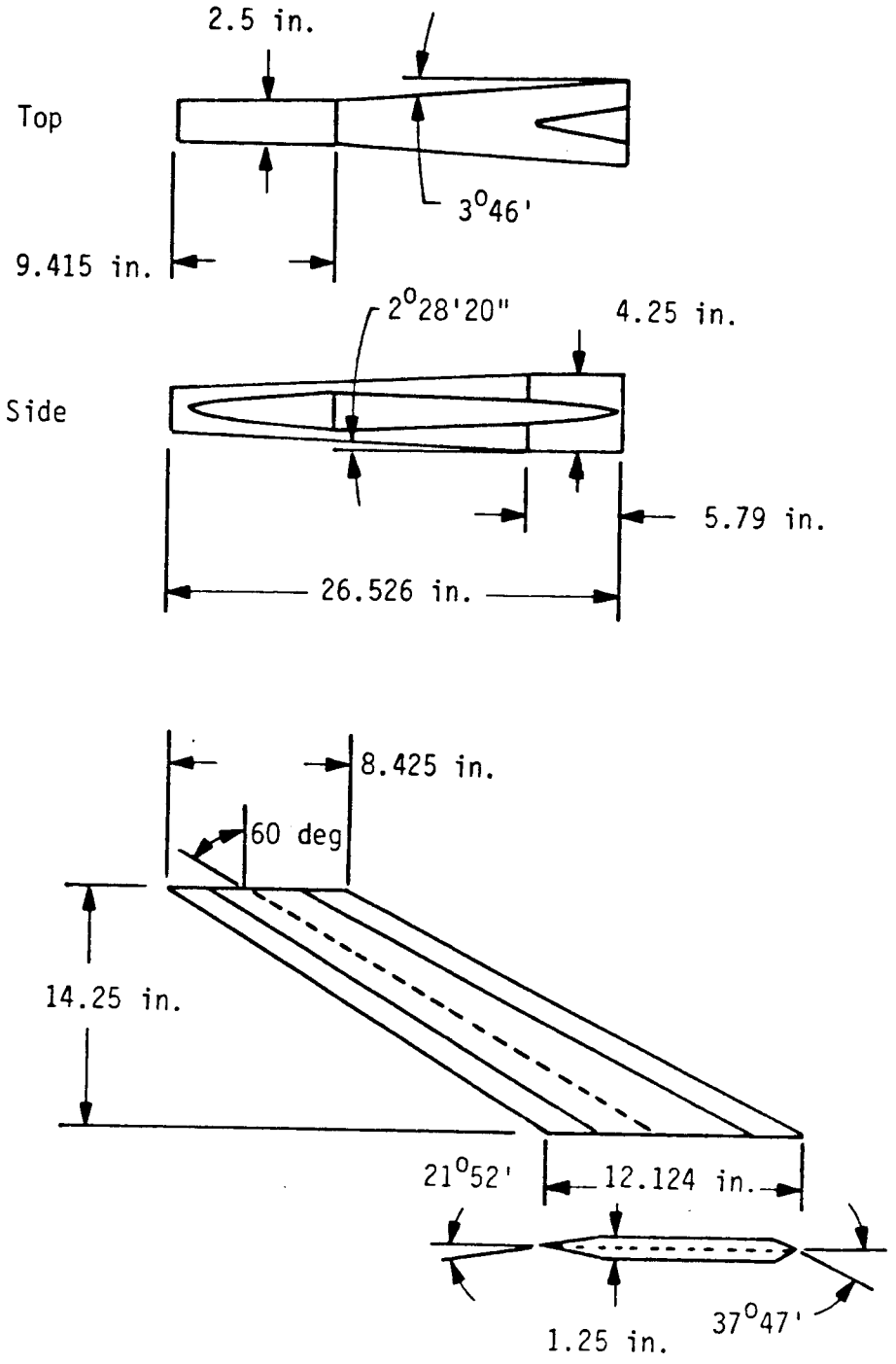


Figure 3. Support Configurations



Note: Upper blade indentical to lower blade

Figure 4. Sting and Blade Support Hardware Details

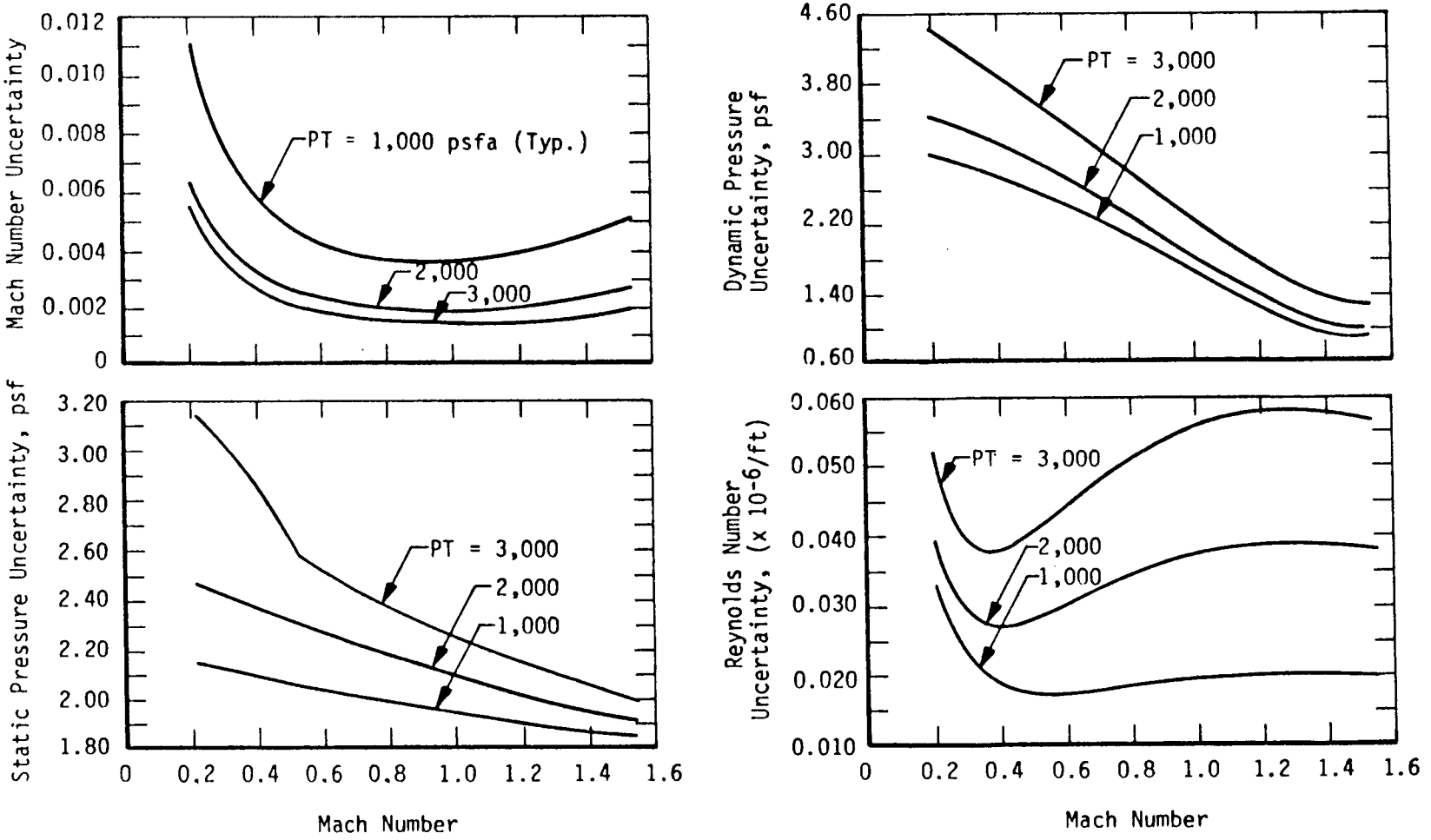
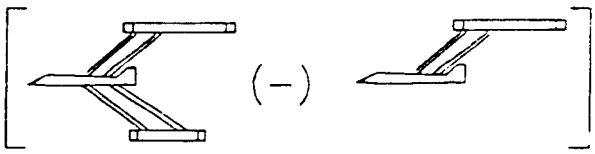
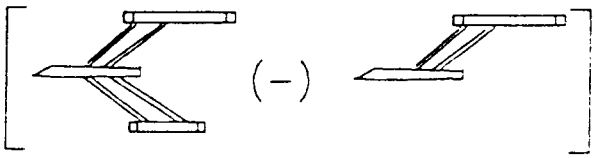


Figure 5. Uncertainties of Basic Wind Tunnel Parameters

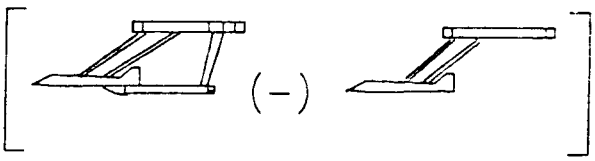
Lower Blade Tail On



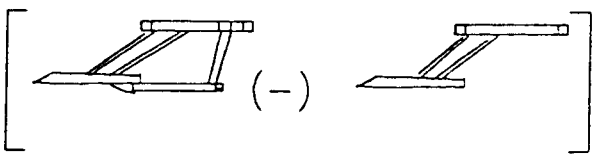
Lower Blade Tail Off



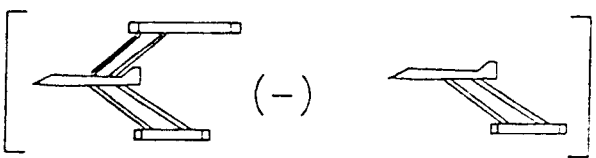
Sting Tail On



Sting Tail Off



Upper Blade Tail On



Upper Blade Tail Off

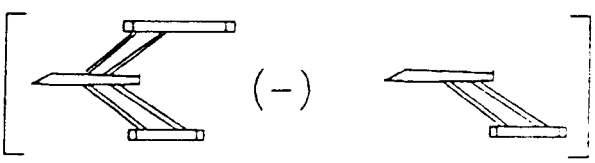
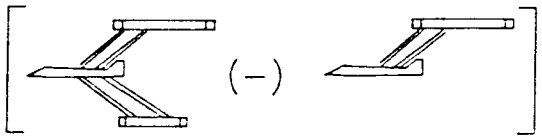
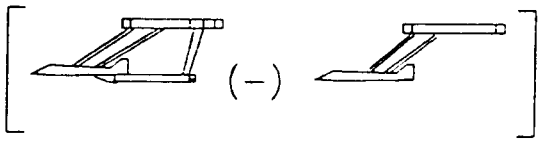


Figure 6. Support Increments

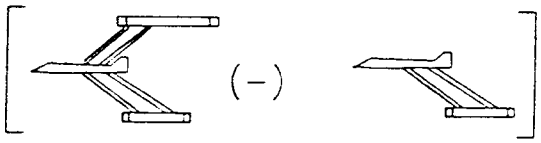
■ Lower Blade Tail On



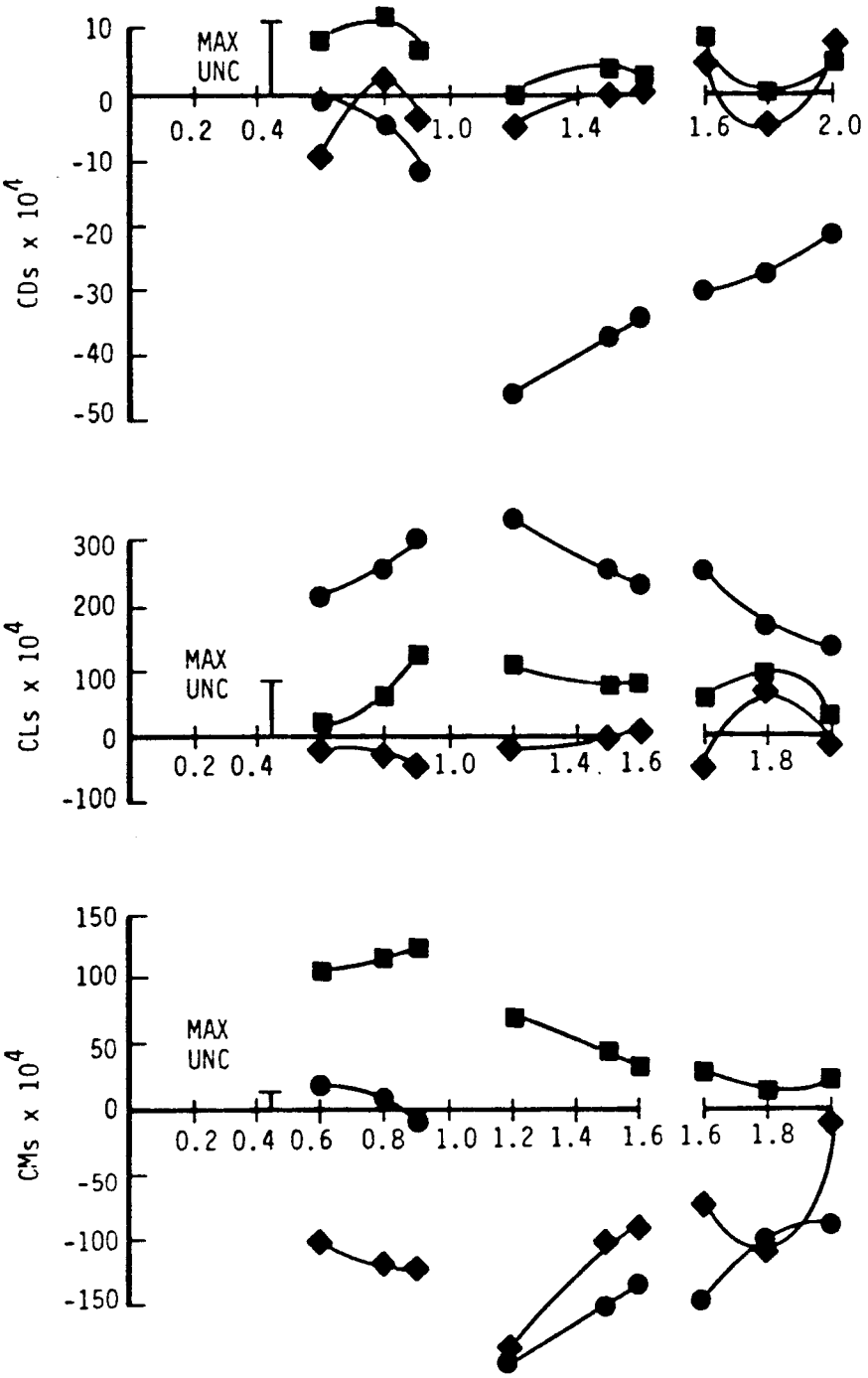
● Sting Tail On



◆ Upper Blade Tail On



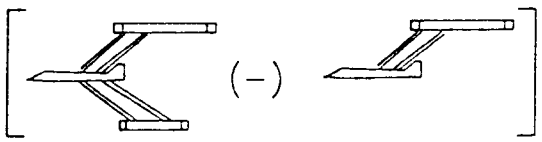
Legend for Figure 7a



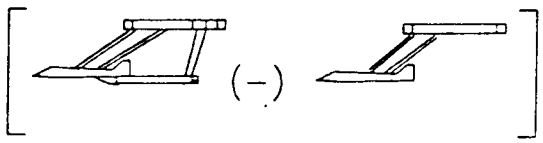
a. Alpha = -2 deg

Figure 7. Comparison of Support Effects, Tail On

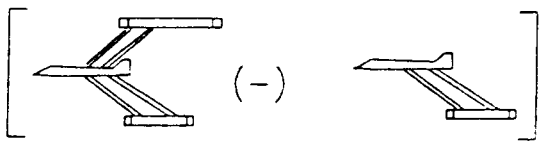
■ Lower Blade Tail On



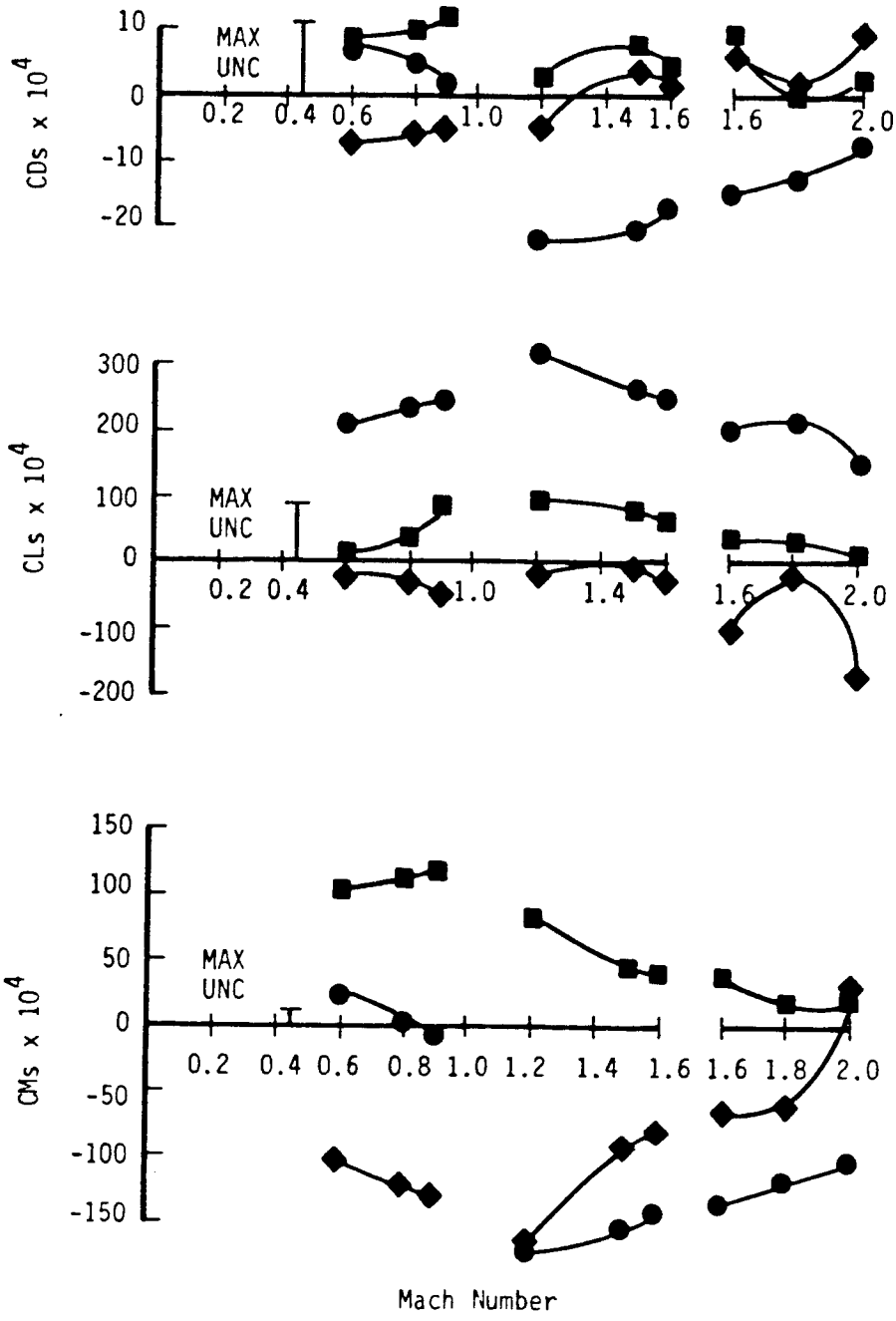
● Sting Tail On



◆ Upper Blade Tail On



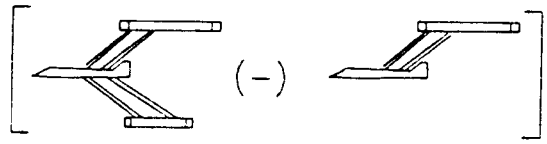
Legend for Figure 7b



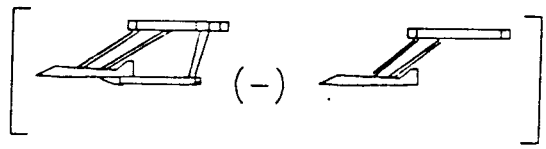
b. Alpha = 0 deg

Figure 7. Continued

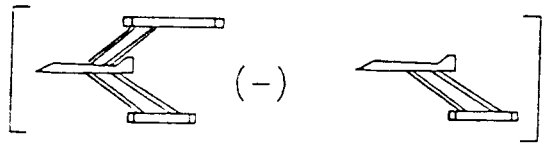
■ Lower Blade Tail On



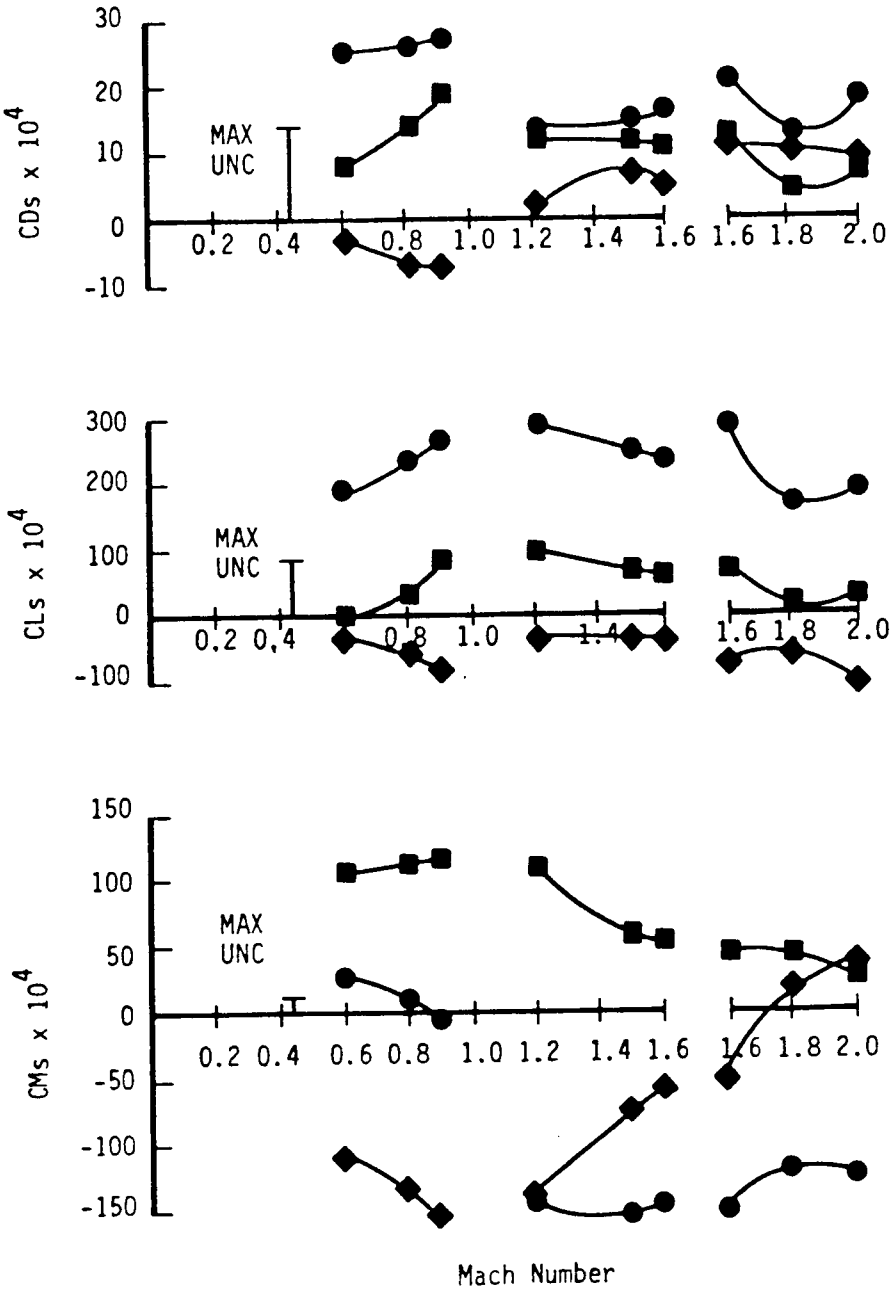
● Sting Tail On



◆ Upper Blade Tail On



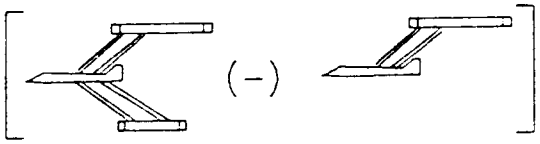
Legend for Figure 7c



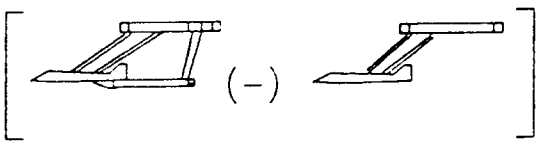
c. Alpha = 4 deg

Figure 7. Continued

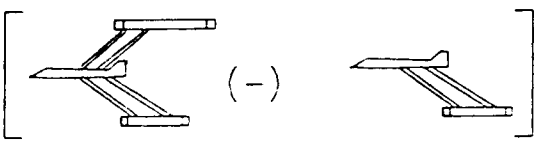
■ Lower Blade Tail On



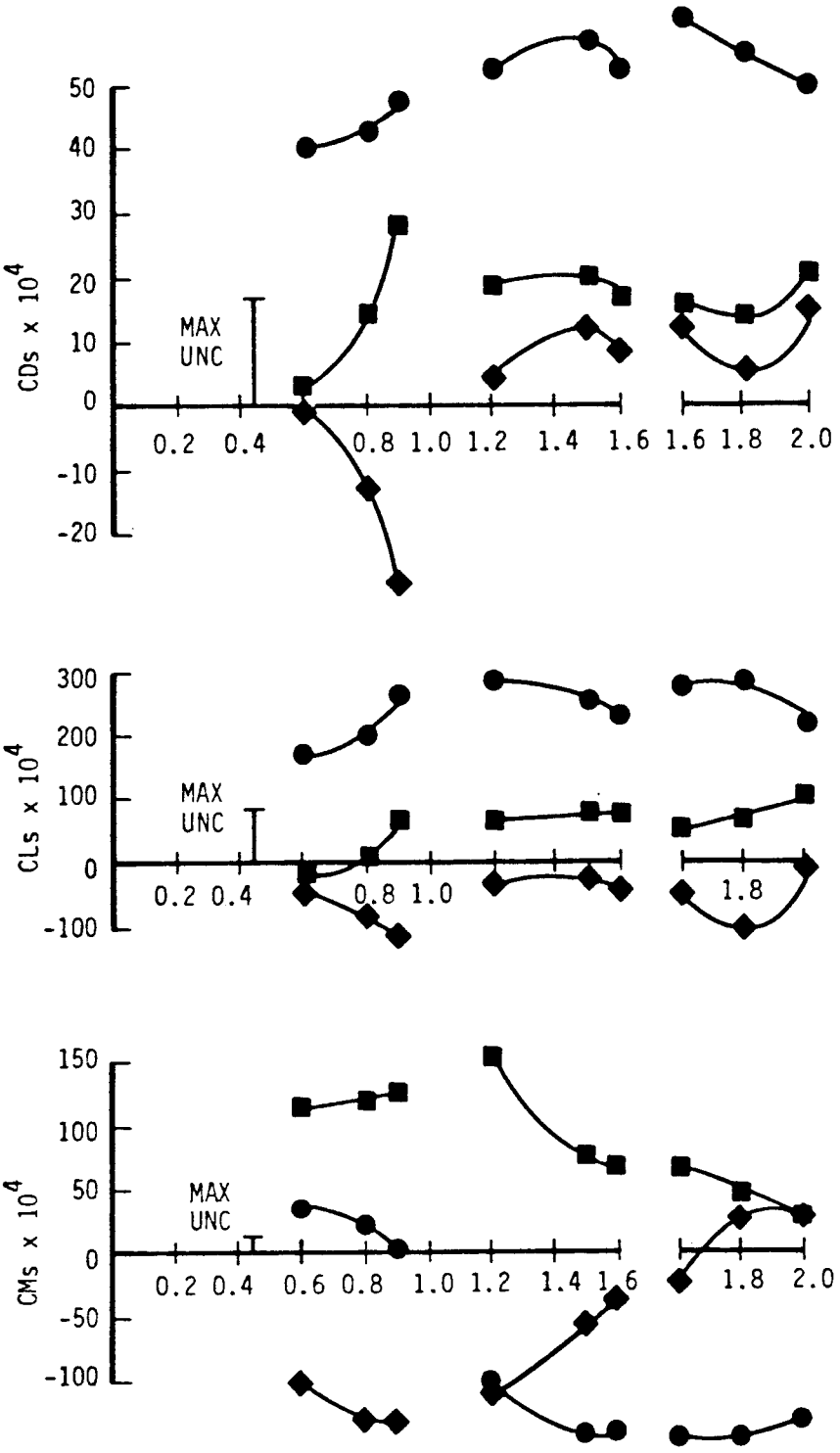
● Sting Tail On



◆ Upper Blade Tail On



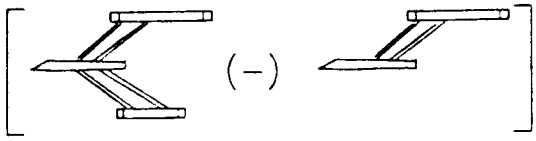
Legend for Figure 7d



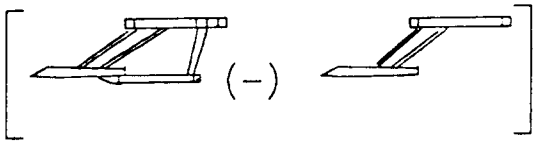
d. Alpha = 8 deg

Figure 7. Concluded

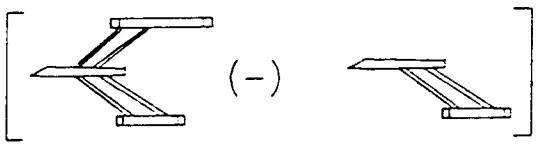
□ Lower Blade Tail On



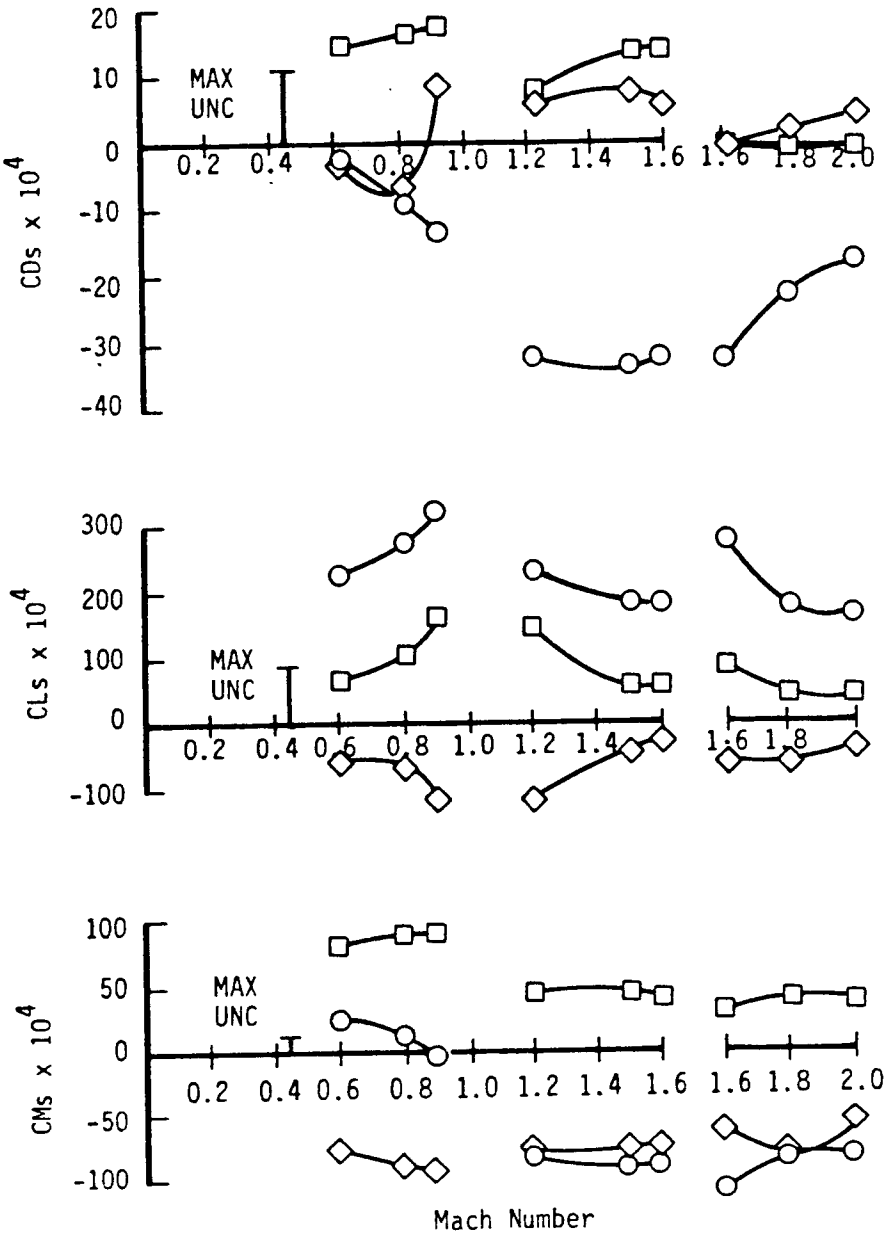
○ Sting Tail On



◇ Upper Blade Tail On



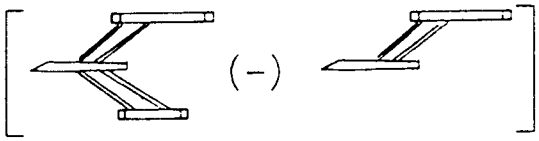
Legend for Figure 8a



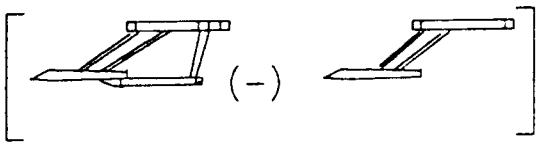
a. Alpha = -2 deg

Figure 8. Comparison of Support Effects, Tail Off

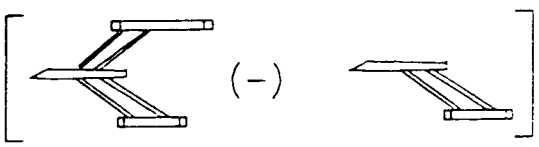
□ Lower Blade Tail Off



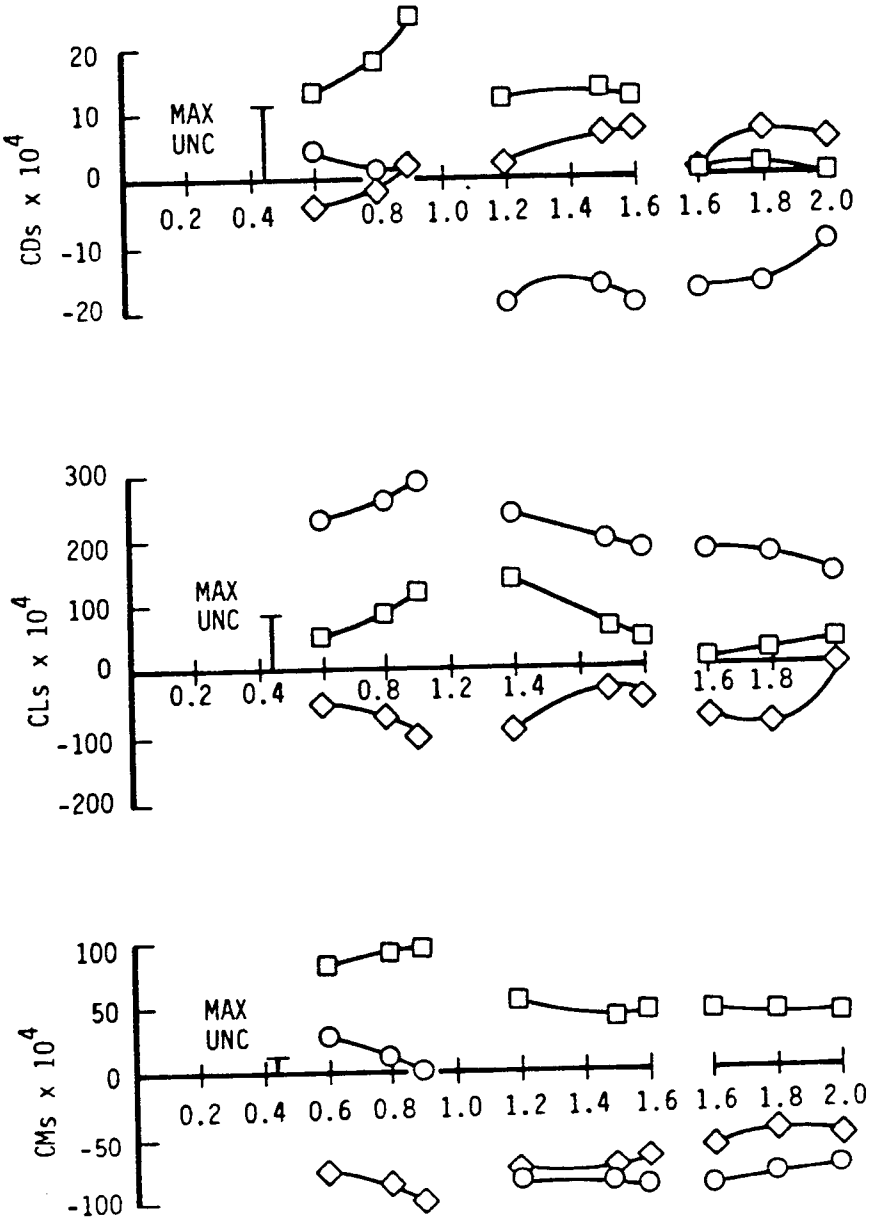
○ Sting Tail Off



◇ Upper Blade Tail Off



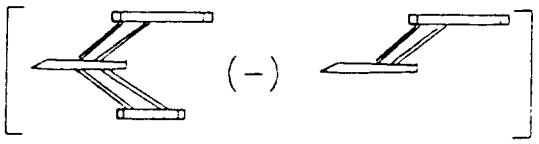
Legend for Figure 8b



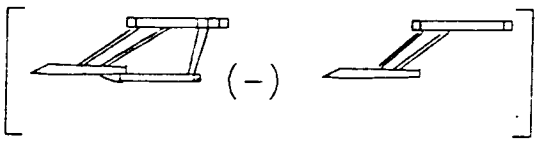
b. Alpha = 0 deg

Figure 8. Continued

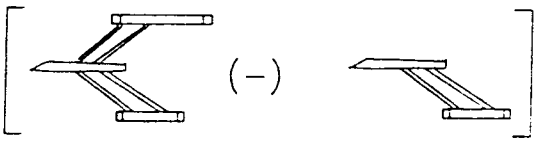
□ Lower Blade Tail Off



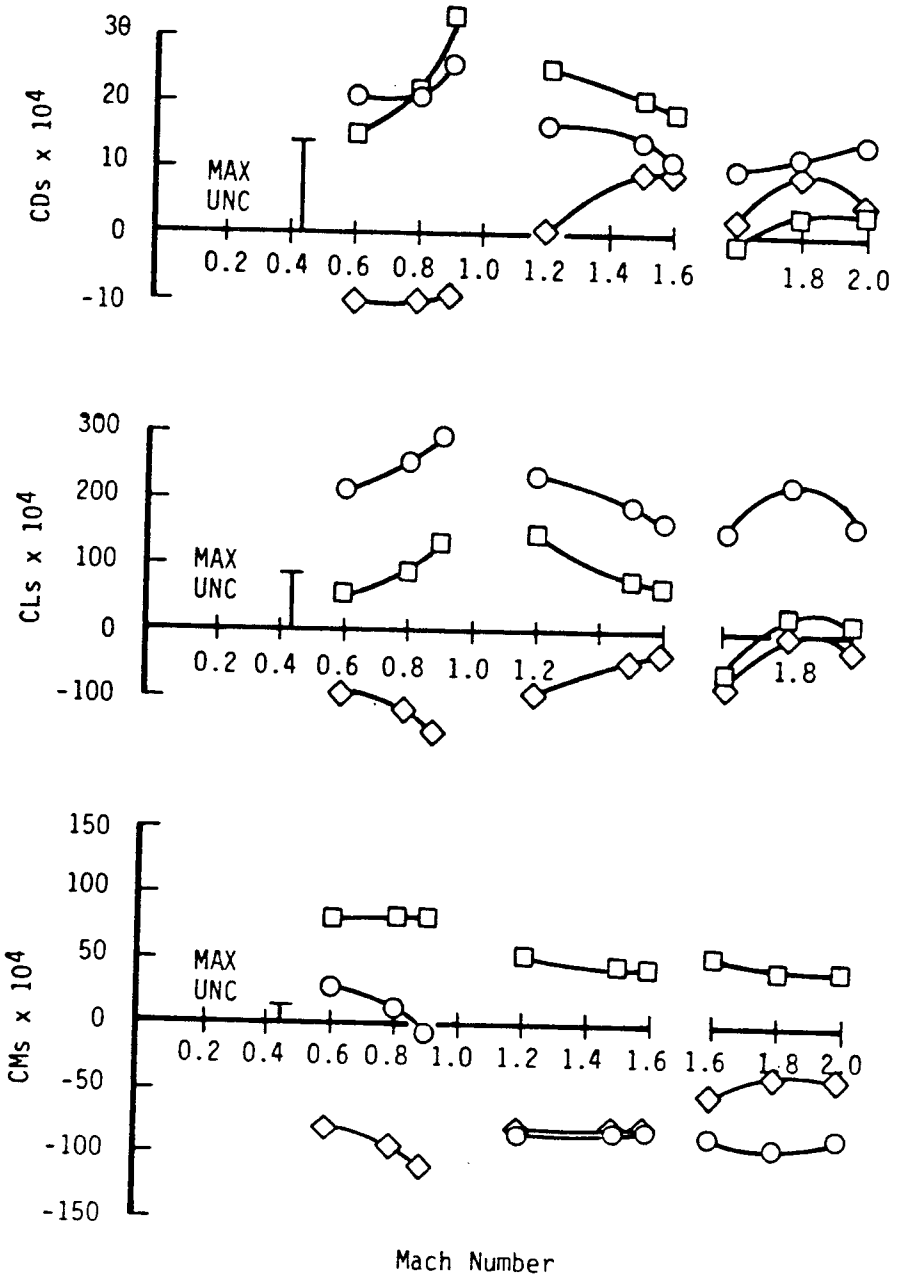
○ Sting Tail Off



◇ Upper Blade Tail Off



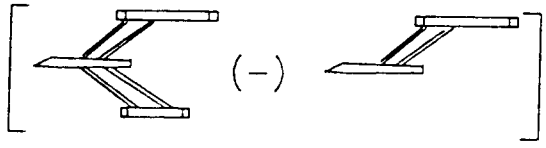
Legend for Figure 8c



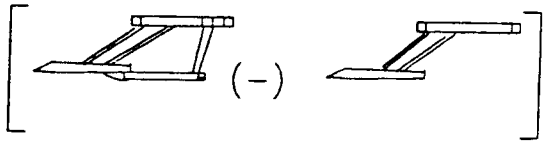
c. Alpha = 4 deg

Figure 8. Continued

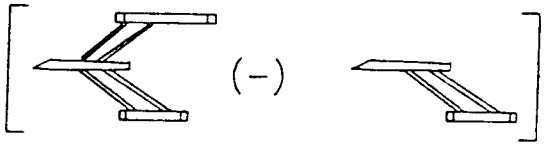
□ Lower Blade Tail Off



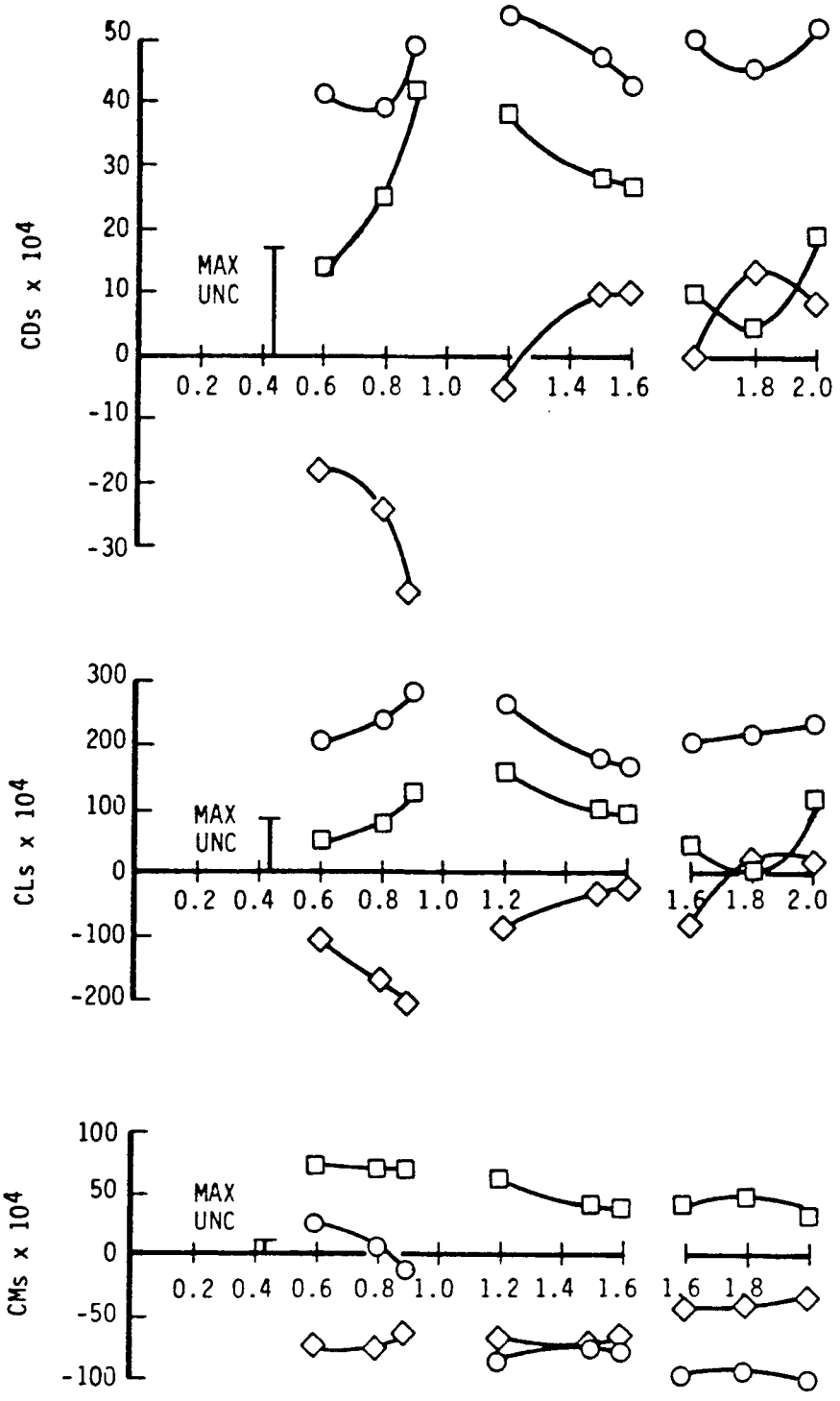
○ Sting Tail Off



◇ Upper Blade Tail Off



Legend for Figure 8d



d. Alpha = 8 deg

Figure 8. Concluded

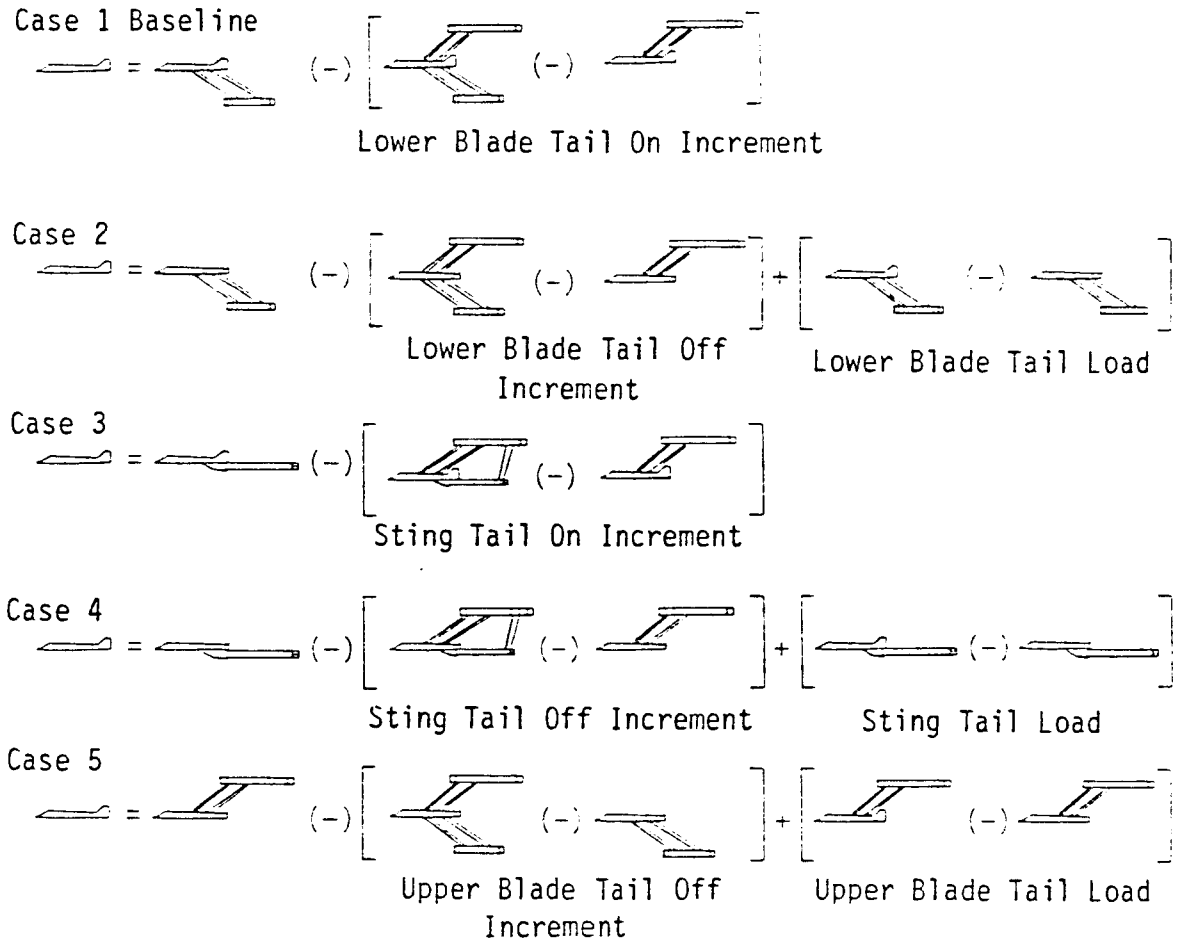
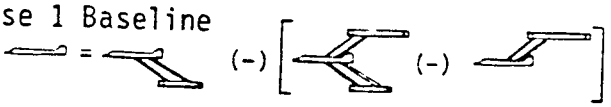


Figure 9. Support Correction Methodology

[Ref.]

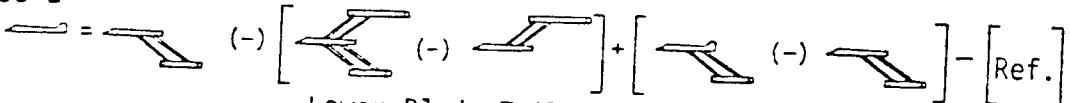
Case 1 Baseline



Lower Blade Tail On Increment

□

Case 2



Lower Blade Tail Off Increment

Lower Blade Tail Load

●

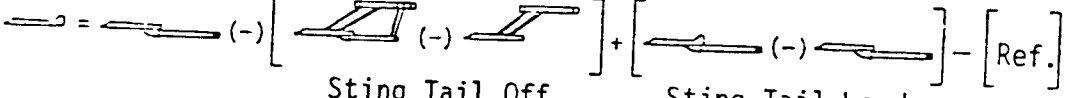
Case 3



Sting Tail On Increment

○

Case 4



Sting Tail Off Increment

Sting Tail Load

◇

Case 5

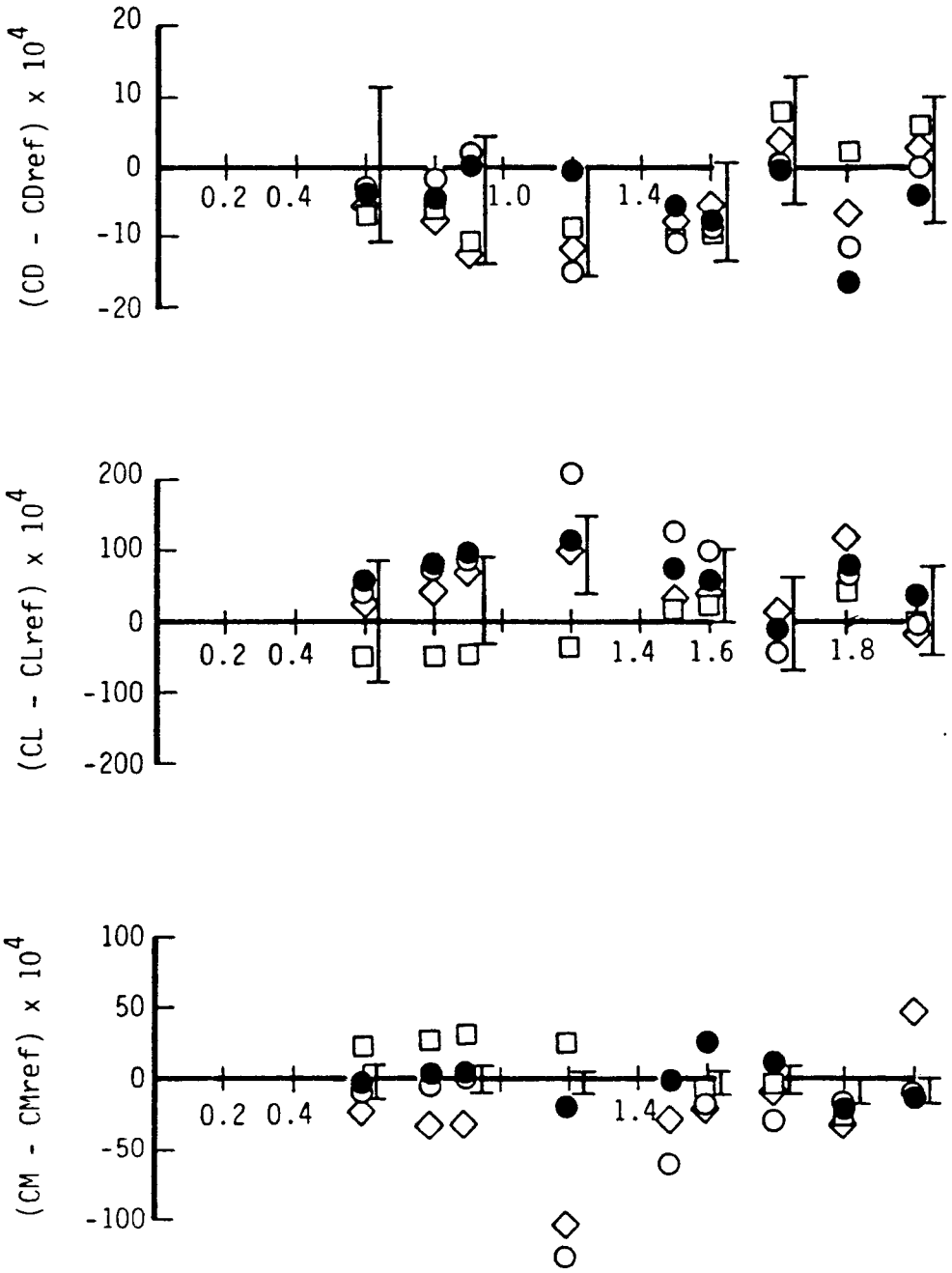


Upper Blade Tail Off Increment

Upper Blade Tail Load

I Uncertainty Band (± the Uncertainty)

Legend for Figure 10a

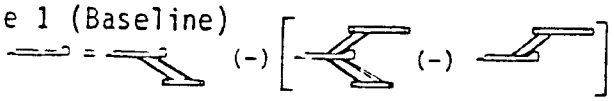


a. Alpha = -2 deg

Figure 10. Comparison of Corrections

[Ref.]

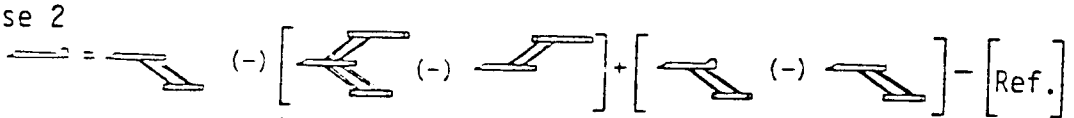
Case 1 (Baseline)



Lower Blade Tail On Increment

□

Case 2



Lower Blade Tail Off Lower Blade Tail Load

●

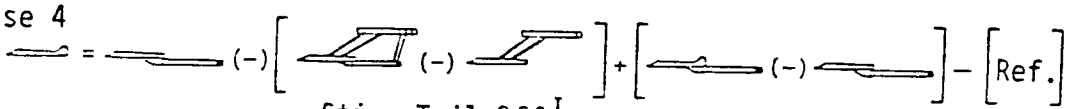
Case 3



Sting Tail On Increment

○

Case 4



Sting Tail Off Increment Sting Tail Load

◇

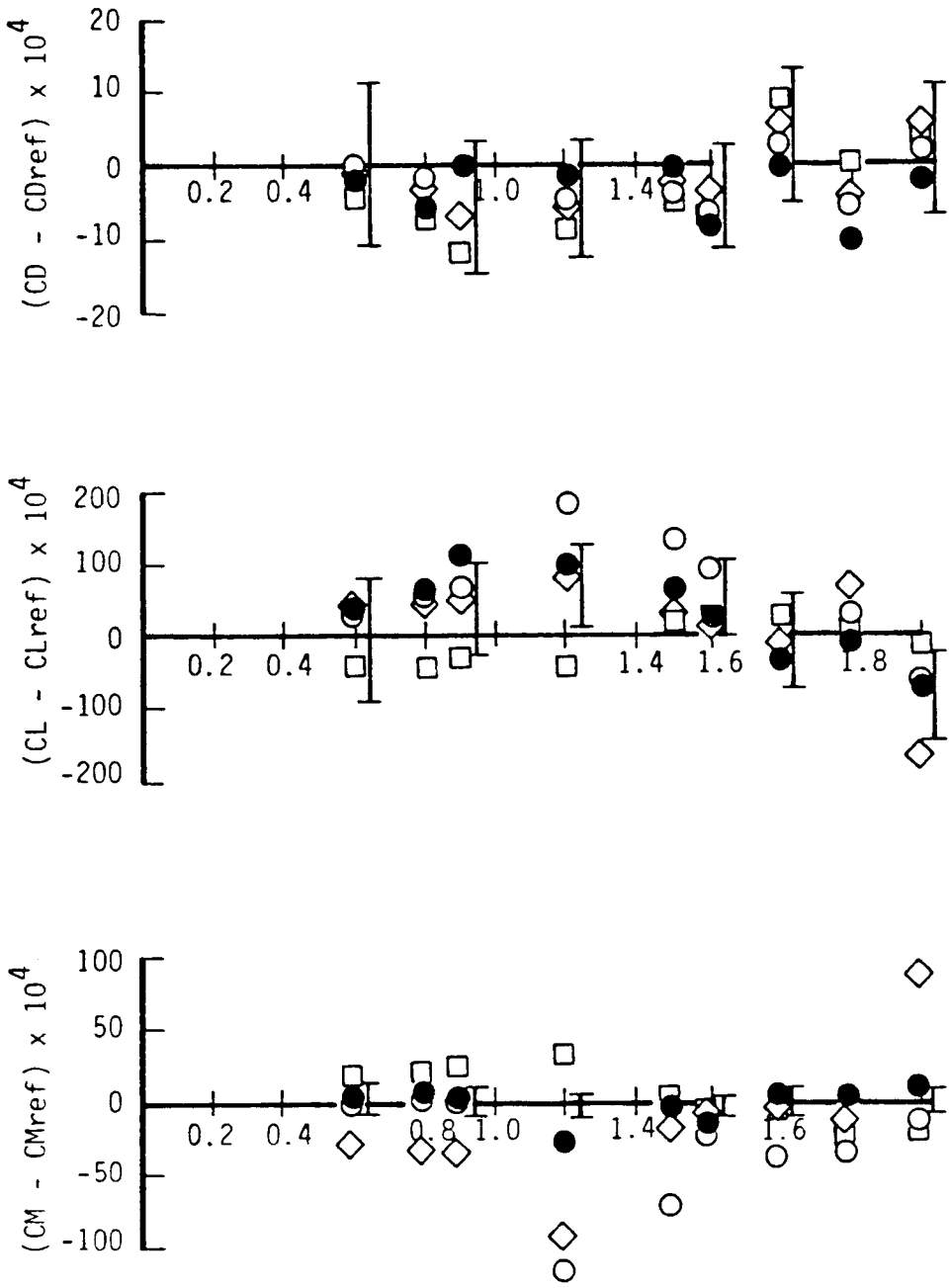
Case 5



Upper Blade Tail Off Increment Upper Blade Tail Load

I Uncertainty Band (± the Uncertainty)

Legend for Figure 10b

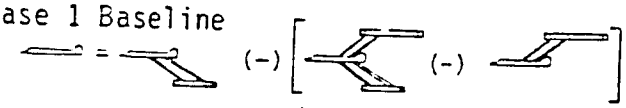


b. Alpha = 0 deg

Figure 10. Continued

[Ref.]

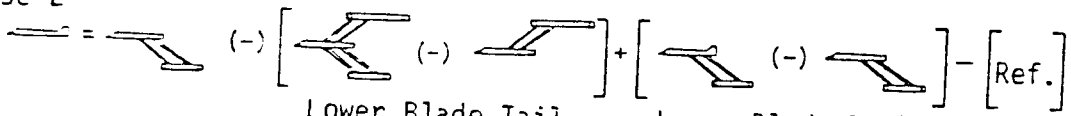
Case 1 Baseline



Lower Blade Tail On Increment

□

Case 2



Lower Blade Tail Off Increment

Lower Blade Tail Load

●

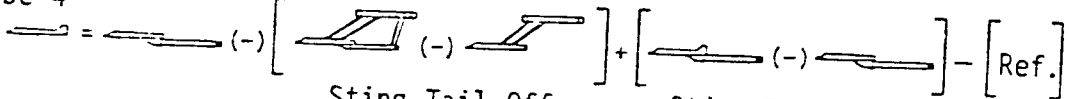
Case 3



Sting Tail On Increment

○

Case 4

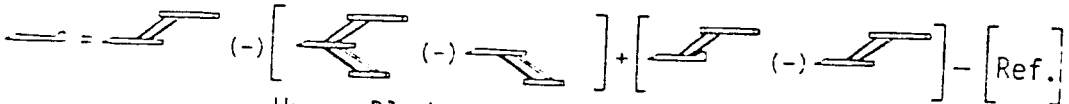


Sting Tail Off Increment

Sting Tail Load

◇

Case 5

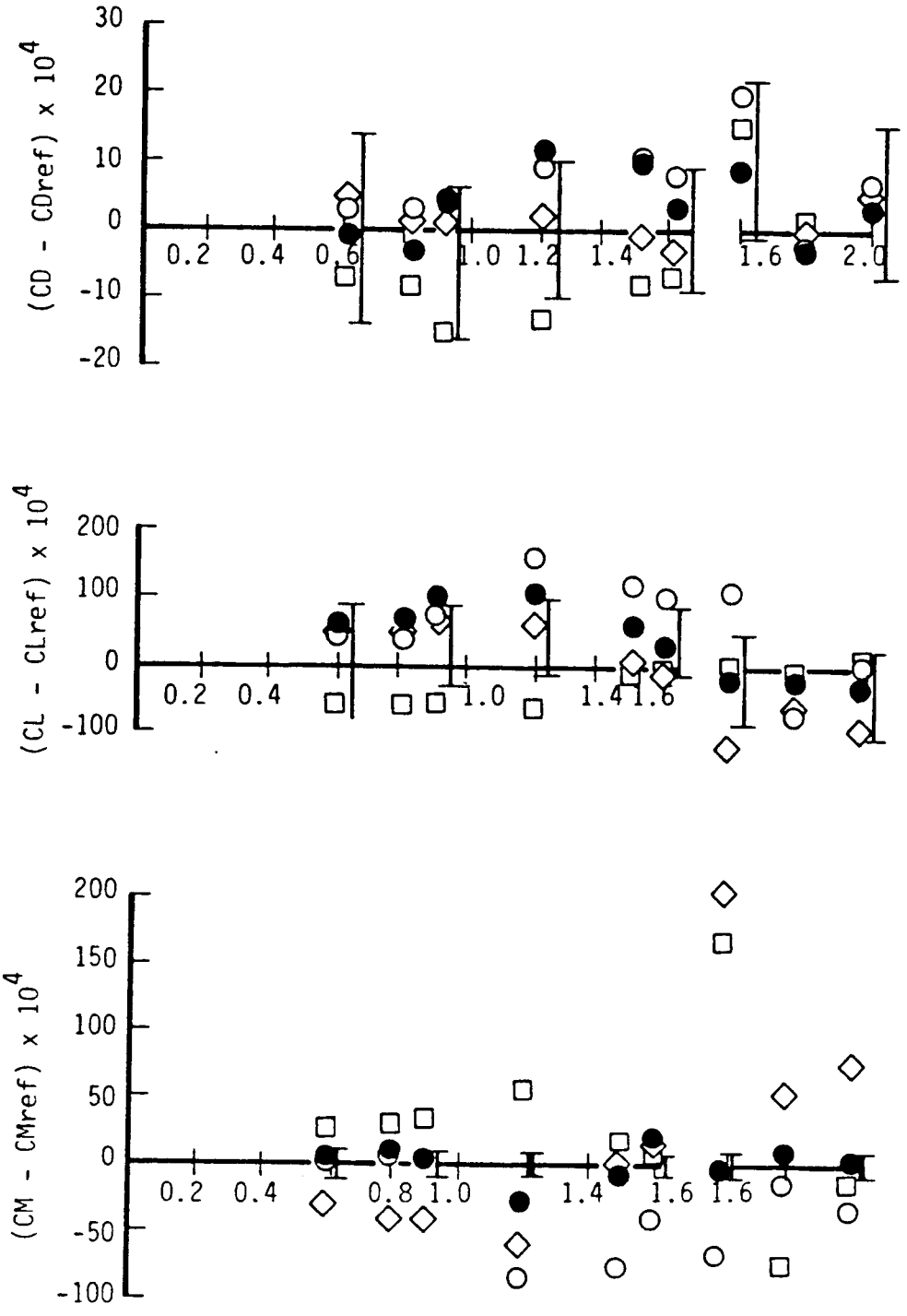


Upper Blade Tail Off Increment

Upper Blade Tail Load

I Uncertainty Band (± the Uncertainty)

Legend for Figure 10c

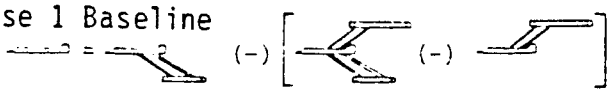


c. Alpha = 4 deg

Figure 10. Continued

[Ref.]

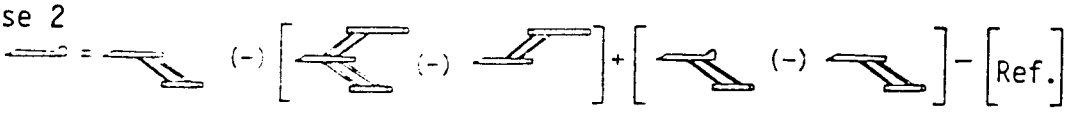
Case 1 Baseline



Lower Blade Tail On Increment

□

Case 2



Lower Blade Tail Off Increment

Lower Blade Tail Load

●

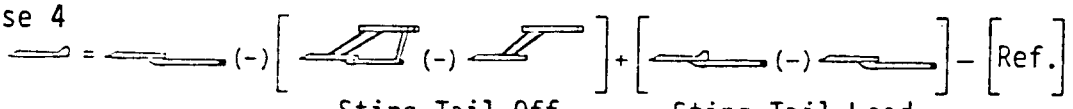
Case 3



Sting Tail On Increment

○

Case 4

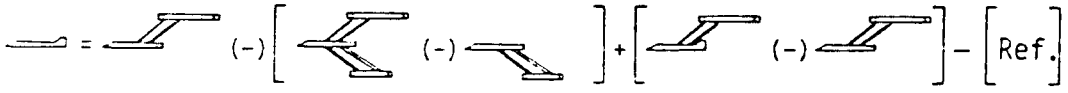


Sting Tail Off Increment

Sting Tail Load

◇

Case 5

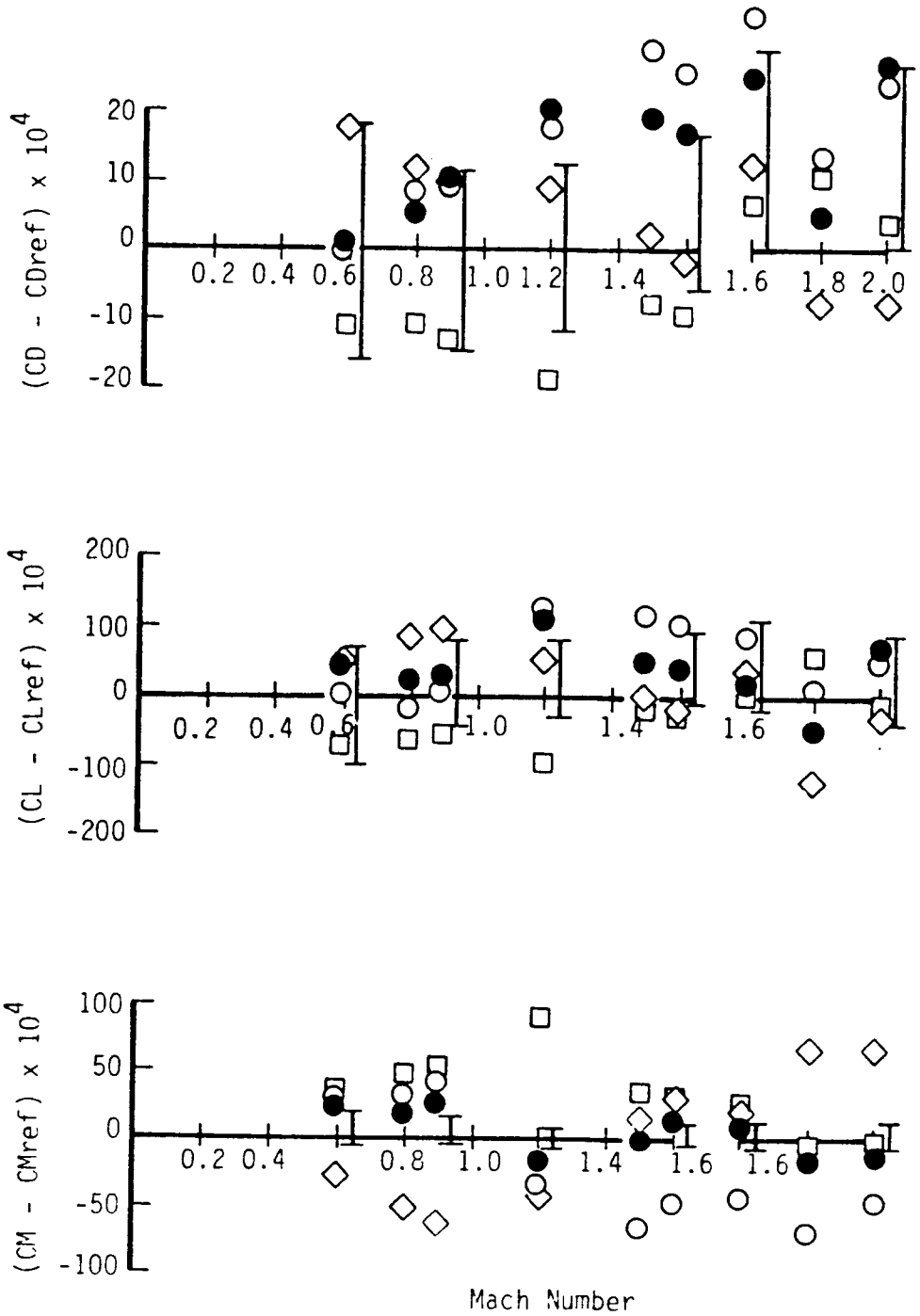


Upper Blade Tail Off Increment

Upper Blade Tail Load

I Uncertainty Band (± the Uncertainty)

Legend for Figure 10d



d. Alpha = 8 deg

Figure 10. Concluded

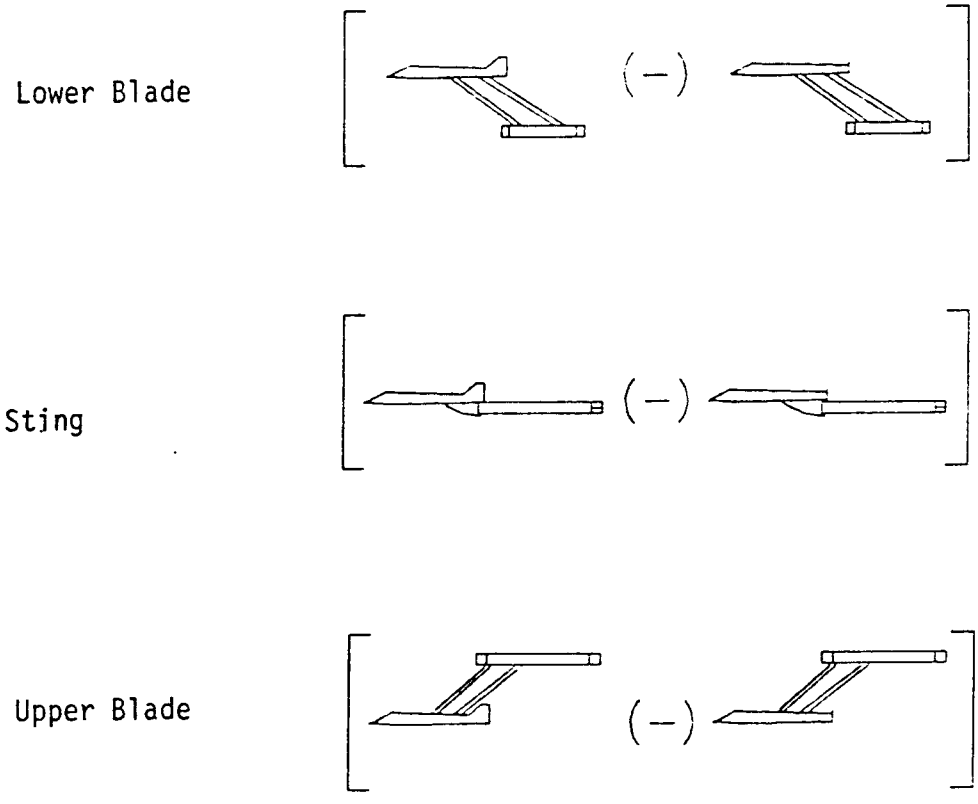
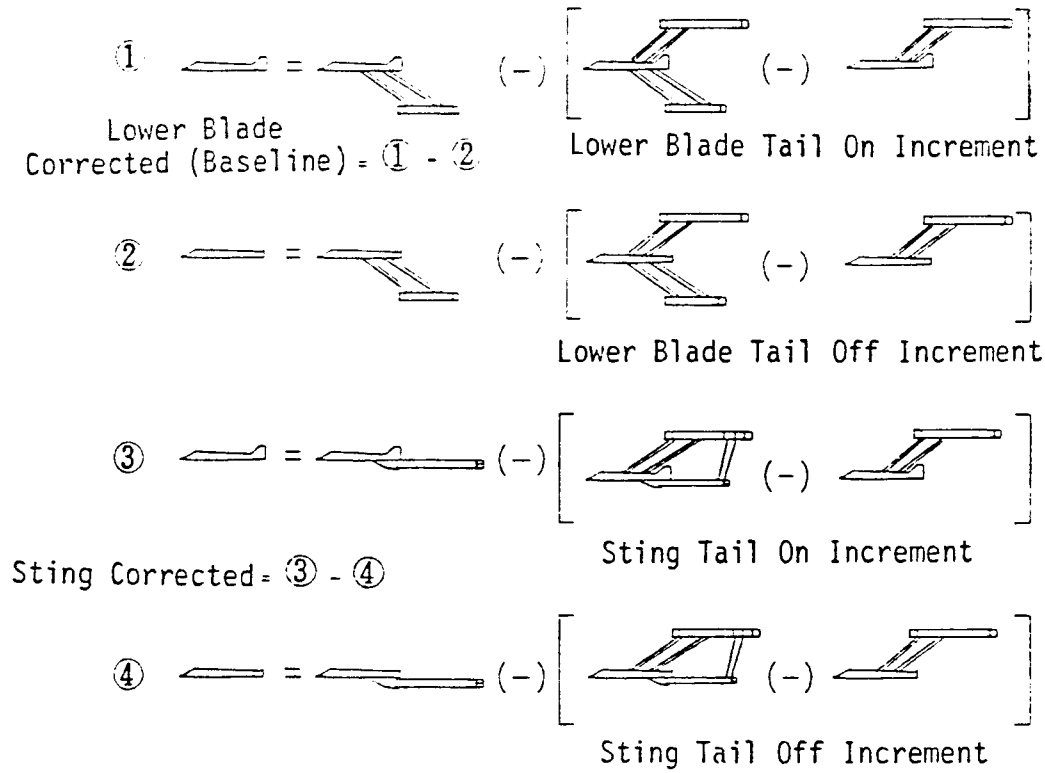
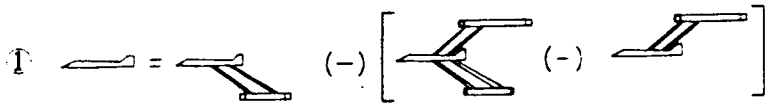


Figure 11. Tail Loads Determination

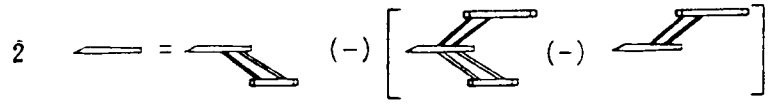


Note: Upper Blade, Corrected is redundant (identical to Lower Blade, Corrected)

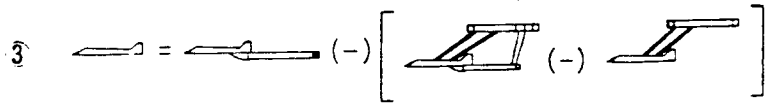
Figure 12. Tail Loads Correction Methodology



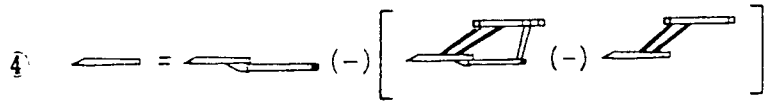
Lower Blade Tail On Increment



Lower Blade Tail Off Increment



Sting Tail On Increment



Sting Tail Off Increment

[Ref.] = Lower Blade Corrected = ①-②

● Sting Corrected = ③-④ − [Ref.]

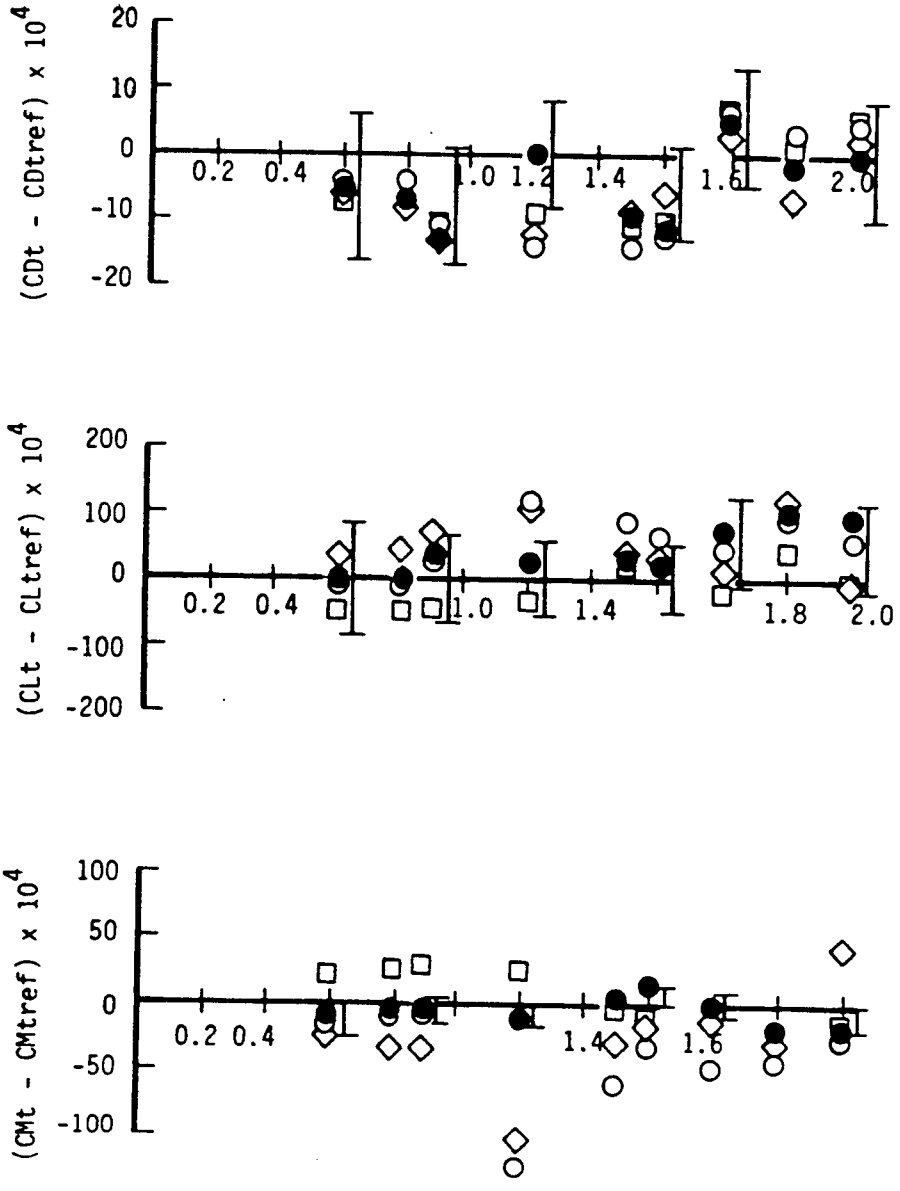
□ Lower Blade [(-)] − [Ref.]

○ Sting [(-)] − [Ref.]

◇ Upper Blade [(-)] − [Ref.]

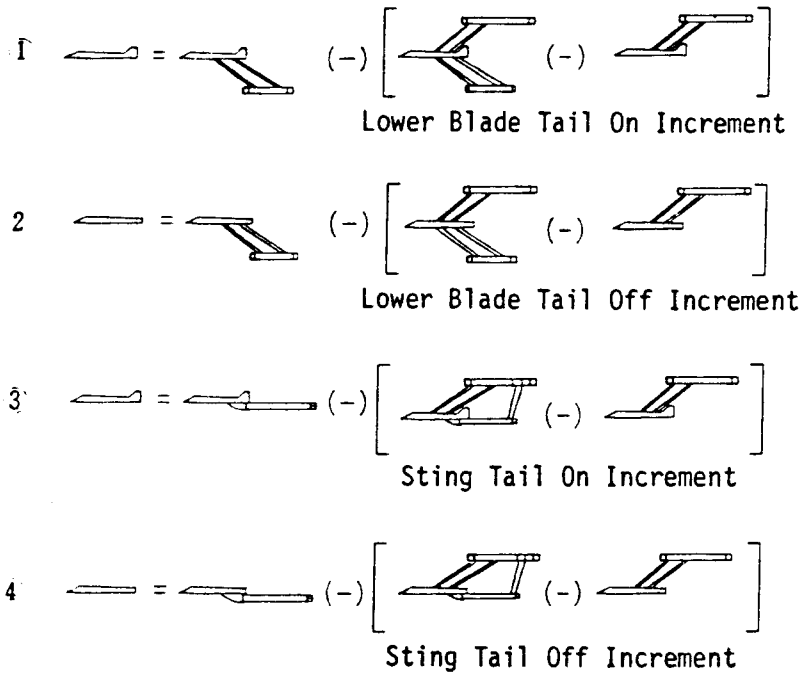
I Uncertainty Band (± the Uncertainty)

Legend for Figure 13a

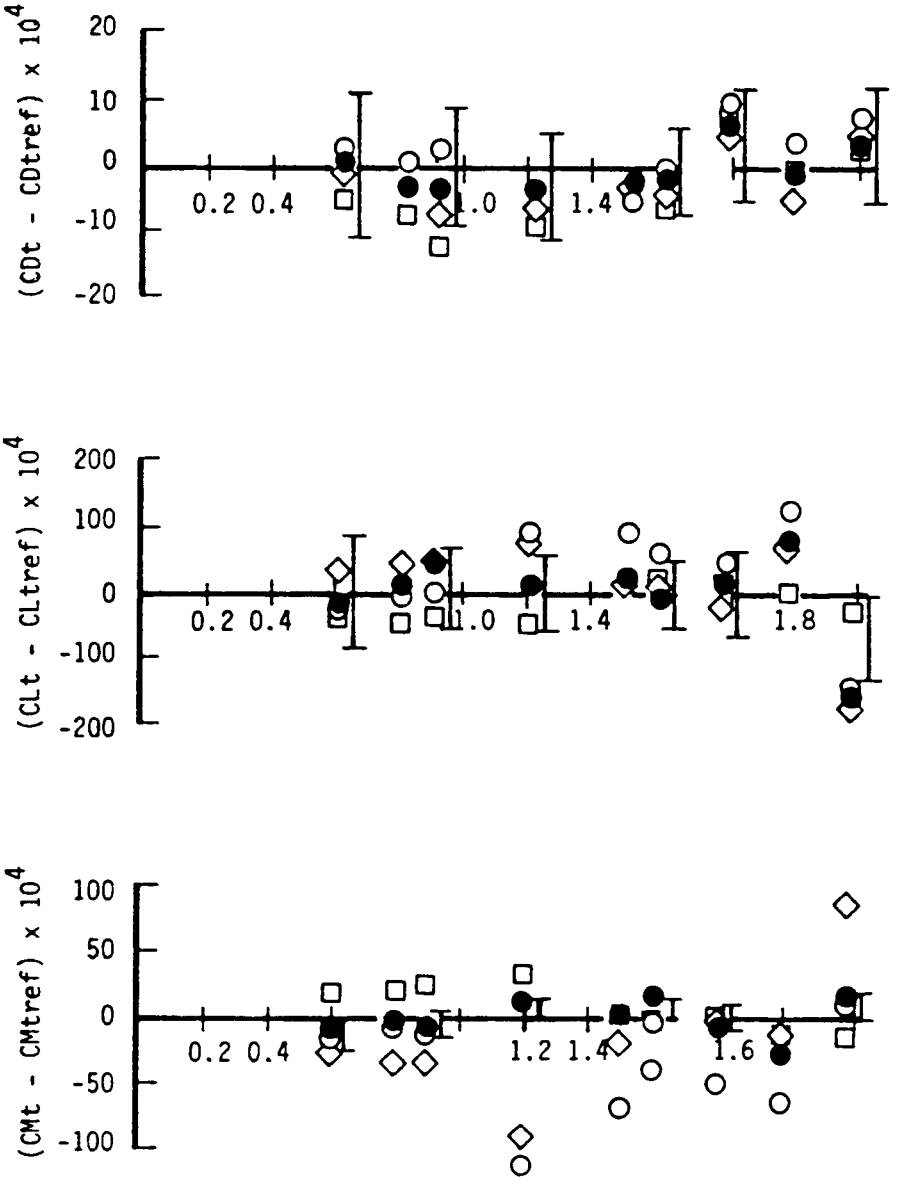


a. Alpha = -2 deg

Figure 13. Comparison of Tail Loads and Corrections

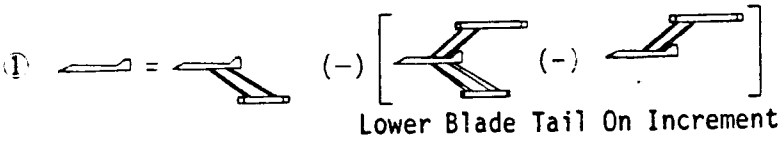


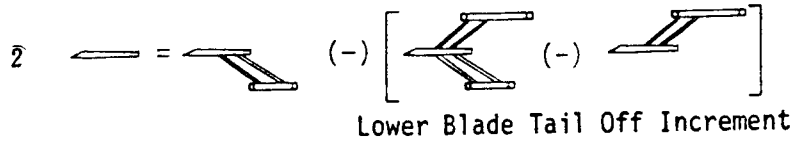
Legend for Figure 13b

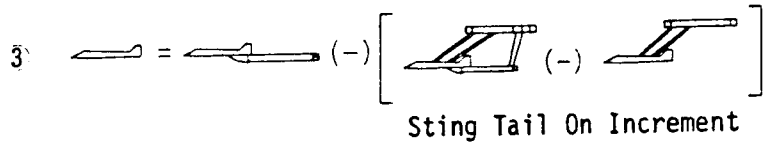


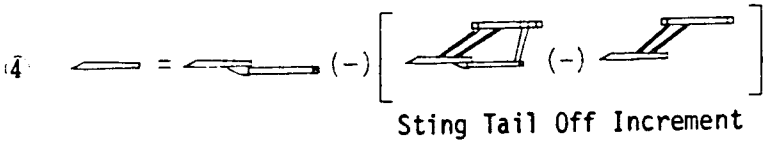
b. Alpha = 0 deg

Figure 13. Continued









[Ref.] = Lower Blade Corrected = ① - ②

● Sting Corrected = ③ - ④ − [Ref.]

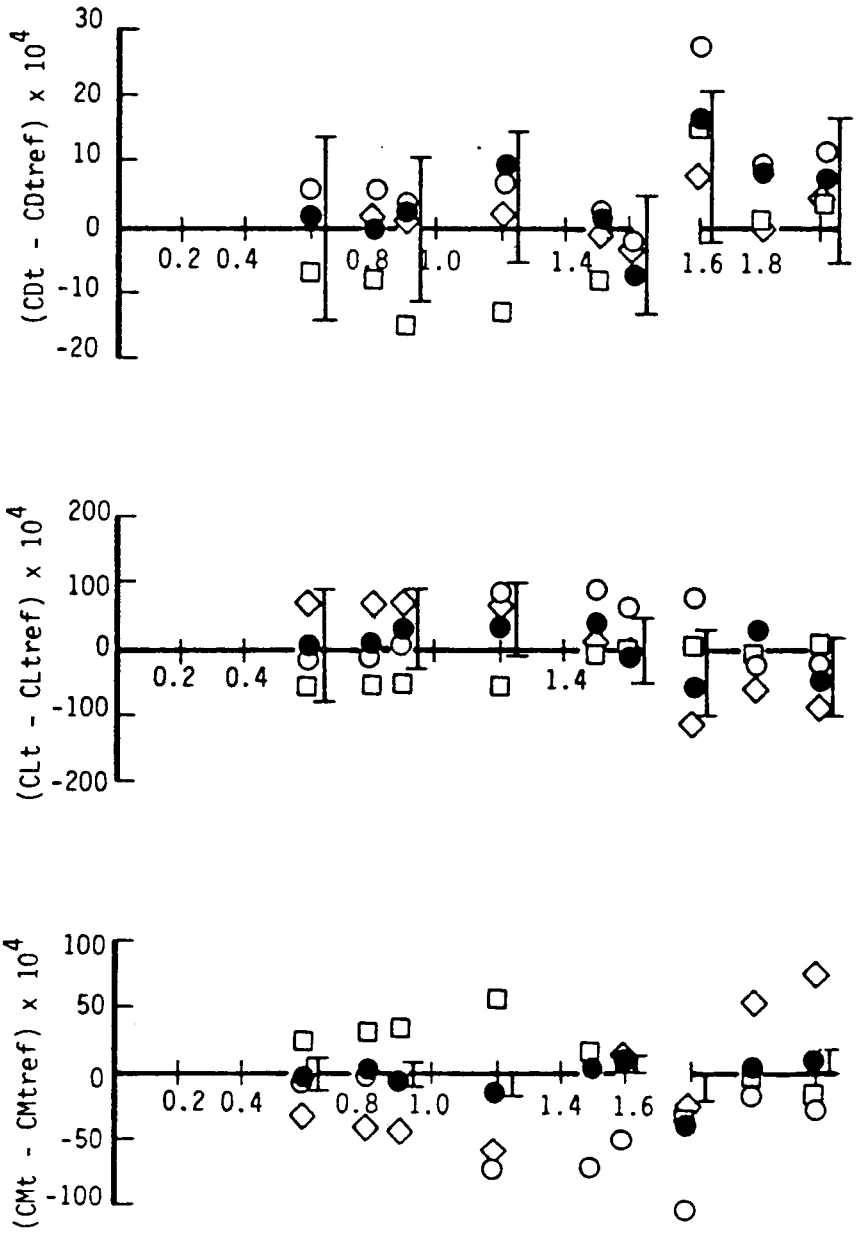
□ Lower Blade [(-)] − [Ref.]

○ Sting [(-)] − [Ref.]

◇ Upper Blade [(-)] − [Ref.]

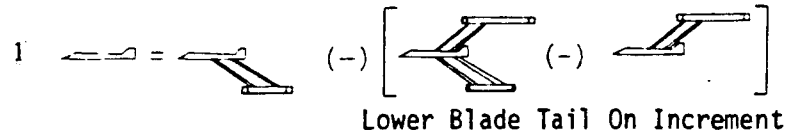
I Uncertainty Band (± the Uncertainty)

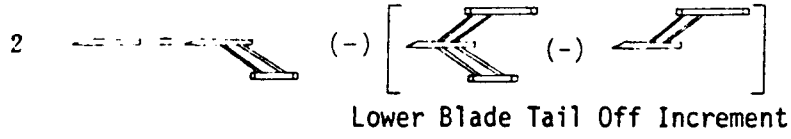
Legend for Figure 13c

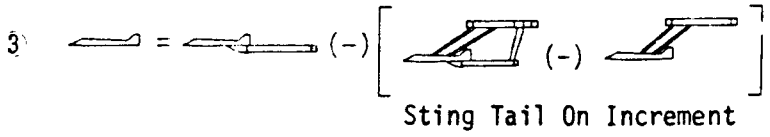


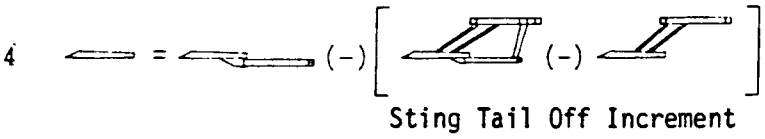
c. Alpha = 4 deg

Figure 13. Continued









[Ref.] = Lower Blade Corrected = ①-②

● Sting Corrected = ③-④ – [Ref.]

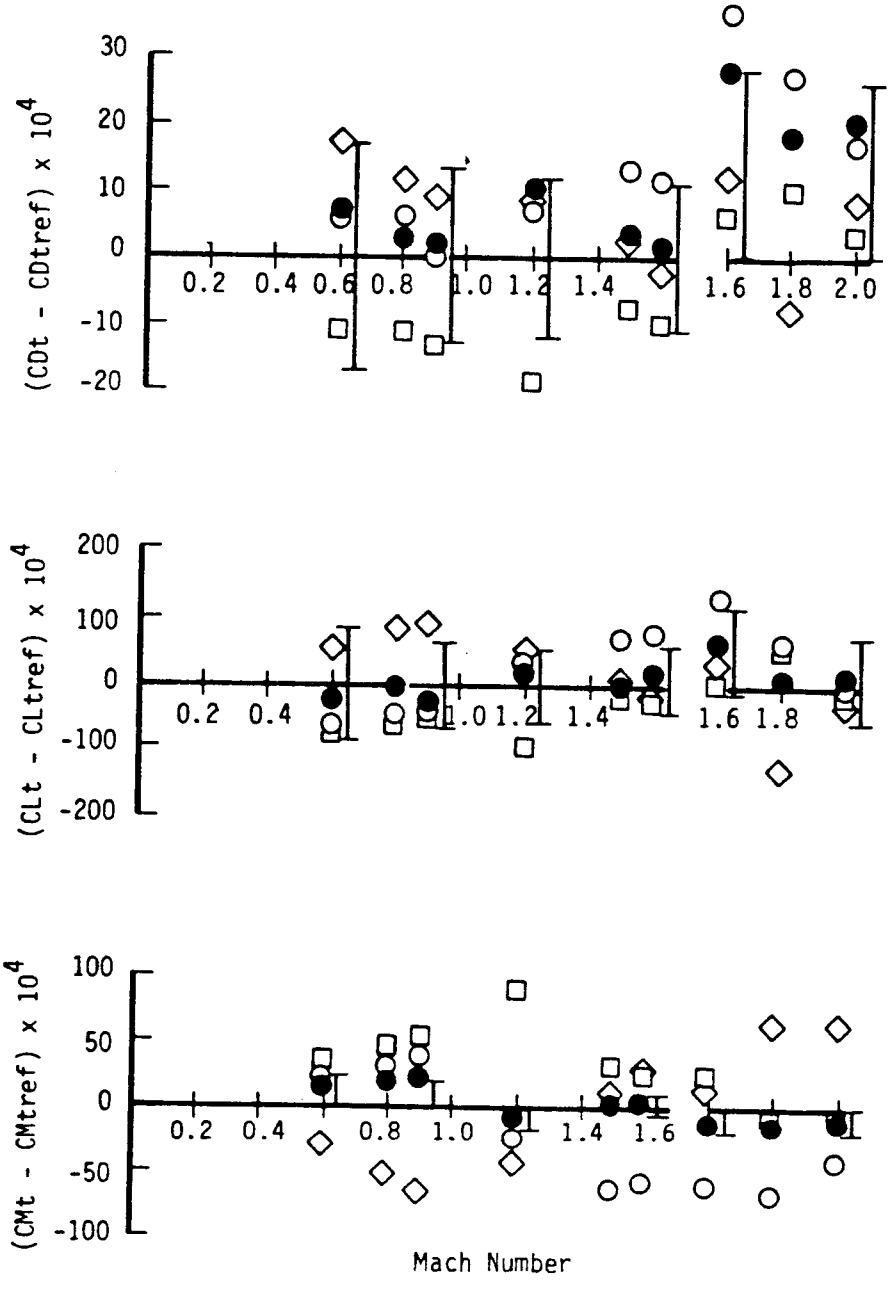
□ Lower Blade [(-)] – [Ref.]

○ Sting [(-)] – [Ref.]

◇ Upper Blade [(-)] – [Ref.]

I Uncertainty Band (± the Uncertainty)

Legend for Figure 13d



d. Alpha = 8 deg

Figure 13. Concluded

APPENDIX B

TABLES

This appendix presents Tables 1 and 2 cited in the main text.

Table 1. Estimated Uncertainties of Basic Test Parameters

Tunnel	Config	M	Alpha Deg	UAlpha Deg	UCD x10^4	UCL x10^4	UCM x10^4
Transonic	L BLADE	0.6	0.0	0.052	11	85	12
Transonic	L BLADE	0.6	8.0	0.052	17	84	12
Transonic	L BLADE	0.9	0.0	0.052	9	63	9
Transonic	L BLADE	0.9	8.0	0.052	13	63	9
Transonic	L BLADE	1.2	0.0	0.052	8	55	8
Transonic	L BLADE	1.2	8.0	0.052	12	55	8
Transonic	L BLADE	1.6	0.0	0.052	7	51	7
Transonic	L BLADE	1.6	8.0	0.052	11	51	7
Supersonic	L BLADE	1.6	0.0	0.052	9	65	9
Supersonic	L BLADE	1.6	8.0	0.052	14	65	9
Supersonic	L BLADE	2.0	0.0	0.052	9	66	9
Supersonic	L BLADE	2.0	8.0	0.052	13	66	9
Transonic	U BLADE	0.9	0.0	0.052	9	63	9
Transonic	STING	0.9	0.0	0.052	9	63	9

Table 2. Repeatability of Basic Test Parameters

M	Alpha Deg	DCDavg x10^4	DCDmax x10^4	DCLavg x10^4	DCLmax x10^4	DCMavg x10^4	DCMmax x10^4	Cond#
0.6	0.0	26	26	3	3	0	0	2
0.6	8.0	5	5	12	12	0	0	2
0.9	0.0	4	9	23	38	2	3	8
0.9	8.0	2	4	7	8	2	2	4
1.2	0.0	1	1	3	4	5	8	6
1.2	8.0	1	1	3	3	2	2	2
1.6 (Transonic)	0.0	6	6	0	0	0	0	2
1.6 (Transonic)	8.0	7	7	7	7	3	3	2
1.6 (Supersonic)	0.0	5	11	18	38	10	20	7
1.6 (Supersonic)	8.0	12	14	49	74	10	18	5
2.0	0.0	3	3	21	21	9	9	2
2.0	8.0	0	0	16	16	5	5	2

VITA

David Whitby was born in Lemore, California, on May 2, 1964. He attended Kempsville High School in Virginia Beach, Virginia. In the fall of 1982, he began his undergraduate work at the Virginia Polytechnic Institute and State University at Blacksburg, Virginia, receiving a Bachelor of Science degree in Aerospace and Ocean Engineering in June 1986.

In May 1986, he accepted a project engineering position with Calspan Corporation at the Arnold Engineering Development Center. During this period he continued his studies on a part-time basis at the University of Tennessee Space Institute at Tullahoma, Tennessee, receiving a Master of Science degree in Aerospace Engineering in August 1989.

Mr. Whitby is married to the former Susan Daniel of Tullahoma, Tennessee.